UNIVERSIDAD NACIONAL AUTÓNOMA DE MÉXICO
PROGRAMA DE MAESTRÍA Y DOCTORADO EN INGENIERÍA
ENERGÍA – SISTEMAS ENERGÉTICOS

NEUTRONIC STUDY OF THE ASTRID SODIUM-COOLED FAST REACTOR WITH THORIUM BASED FUEL

TESIS
QUE PARA OPTAR POR EL GRADO DE:
MAESTRO EN INGENIERÍA

PRESENTA:
DANIEL ESCORCIA ORTIZ

TUTOR PRINCIPAL
DR. JUAN LUIS FRANCOIS LACOUTURE
FACULTAD DE INGENIERÍA

CD. MX., JULIO 2018

JURADO ASIGNADO:

Presidente:	Dr. Espinosa Paredes Gilberto
Secretario:	Dra. Martín del Campo Márquez Cecilia
Vocal:	Dr. Francois Lacouture Juan Luis
1er Suplente:	Dr. Núñez Carrera Alejandro
2do Suplente:	M. en C. Salazar Salazar Edgar

Lugar o lugares donde se realizó la tesis: CIUDAD DE MÉXICO

TUTOR DE TESIS

Dr. Juan Luis Francois Lacouture

FIRMA

Acknowledgements

To the National Autonomous University of Mexico for giving me the opportunity to pursue postgraduate studies. In addition, for its support with the project PAPIIT-IN115517 and for facilitating the use of the MIZTLI supercomputer under the LANCAD-UNAM-DGTIC-253 project.

To the National Council of Science and Technology (CONACYT), for providing economic support for the accomplishment of my master studies.

To the Dr. Juan Luis Francois for sharing his knowledge, and for his commitment and support in the accomplishment of this work.

Abstract

In the present work the utilization of thorium is investigated in the sodium-cooled ASTRID fast reactor core. Two fuel configurations are analyzed: oxide and metallic fuel. Two thorium fueled strategies are analyzed: a mixture of ^{232}Th and ^{233}U in the fertile zone, and both in the fertile and the fissile zone. Both thorium fuel strategies were analyzed in the oxide and in the metallic configurations. To achieve this, the Monte Carlo MCNP6 code with the ENDF/B-VII.0 cross section library was used to perform the calculations. Six neutronic parameters were analyzed for each fuel strategy: the neutron energy spectrum, the effective neutron multiplication factor (keff) for a cycle of 365 days, the shutdown margin, the effective delayed neutron fraction (β_{eff}), the Doppler constant and the reactivity effect of coolant density. The power distribution and the main isotopes evolution were also analyzed. Results show that: The energy spectrum is harder in the metallic fuels and in fuels with very high thorium fraction. The behavior of the keff along the operating cycle in the oxide reference core and with thorium based fuel in the fertile zone is very similar, getting slightly different keff at the end of cycle. The same happens with the metallic reference core and with thorium based fuel in the fertile zone, while these metallic configurations show a less pronounced decrease than the oxide fuels with plutonium. The keff using full ^{232}Th/^{233}U fuel configurations has a significant loss in reactivity, in both the oxide and the metallic configuration, because of their harder spectrum, making them difficult to breed ^{233}U. As in the reference core, ^{239}Pu is bred, the same happens with ^{233}U in the core with thorium based fuel in the fertile zone, in both the oxide and the metallic configuration. This does not happen with full ^{232}Th/^{233}U fuel configurations, as it burns more ^{233}U than it breeds. The Am and Cm actinides concentrations are lower with thorium based fuel in the fertile zone than in the oxide reference core, and are completely absent with full ^{232}Th/^{233}U fuel configurations, in both the metallic and the oxide fuel configurations. They are also lower in the metallic configurations than the oxide configurations. For all the fuel configurations the Doppler constant is negative, it means that the keff drops as the fuel temperature raises, being the core with oxide full ^{232}Th/^{233}U fuel configuration the one with the better performance. Regarding the reactivity effect of coolant density, in general it has a good behavior, as in almost all the studied cases it has a negative reactivity effect, or is low and positive. In the configurations with plutonium, in the case that the fuel region or just the center upper region experience coolant voiding, then a high positive reactivity effect is obtained. Much better performance is obtained with full ^{232}Th/^{233}U fuel configurations, as in all the studied cases they have always a negative, or a very low positive reactivity effect. The power distribution is alike in all core fuel configurations, having a ring with the higher power in the outer fuel region. The full ^{232}Th/^{233}U fuel configurations have the more even power distribution. All fuel configurations have similar β_{eff} and show a good shutdown margin, as it is higher than 1% dk/k at beginning of cycle in all cases.

Resumen

En el presente trabajo se investiga la utilización de torio en el núcleo del reactor rápido refrigerado por sodio ASTRID. Se estudiaron dos configuraciones de combustible: óxido y metálico. Se analizaron dos estrategias de combustible a base de torio: una mezcla de ^{232}Th y ^{233}U en la zona fértil, y en ambas la zona fértil y la zona físil. Las dos estrategias de combustible a base de torio fueron analizadas en las configuraciones de combustible óxido y metálico. Para conseguir esto, se utilizó el código de Monte Carlo MCNP6 con la librería de secciones eficaces ENDF/B-VII.0 para realizar los cálculos. Se analizaron seis parámetros neutrónicos para cada estrategia de combustible: el espectro de energía de neutrones, el factor efectivo de multiplicación de neutrones (keff) para un ciclo de 365 días, el margen de parada, la fracción efectiva de neutrones retardados (β_{eff}), la constante Doppler y el efecto en la reactividad por la densidad del refrigerante. La distribución de potencia y la evolución de isótopos principales también fueron analizados. Los resultados muestran que: el espectro de energía de neutrones es más duro en combustibles metálicos y combustibles con muy alta fracción de torio. El comportamiento de la keff a lo largo del ciclo de operación es muy similar en el núcleo óxido de referencia y el núcleo óxido con combustible basado en torio en la zona fértil, obteniendo una keff ligeramente diferente al final del ciclo. Lo mismo ocurre con el núcleo metálico de referencia y el núcleo metálico con combustible basado en torio en la zona fértil, siendo que estas configuraciones con combustible metálico muestran un descenso menos pronunciado que las configuraciones de combustible óxido con plutonio. La keff usando configuraciones de combustible con ^{232}Th/^{233}U en su totalidad tienen una pérdida significativa de reactividad, en ambas configuraciones óxido y metálico, debido a su espectro endurecido, haciendo difícil la cría de ^{233}U. Así como en el núcleo de referencia se cría ^{239}Pu, lo mismo ocurre con el ^{233}U en el núcleo con combustible a base de torio en la zona fértil, en ambas configuraciones óxido y metálico. Esto no ocurre con las configuraciones de combustible con ^{232}Th/^{233}U en su totalidad, ya que quema más ^{233}U del que produce. Las concentraciones de los actínidos Am y Cm son menores con combustible a base de torio en la zona fértil que en el núcleo de referencia óxido. Y están por completo ausentes en configuraciones de combustible con ^{232}Th/^{233}U en su totalidad, en ambas configuraciones óxido y metálico. También son menores en las configuraciones de combustible metálico que en óxido. Para todas las configuraciones de combustible la constante Doppler es negativa, es decir, que la keff disminuye cuando la temperatura aumenta, siendo el núcleo óxido con combustible con ^{232}Th/^{233}U en su totalidad el que tiene el mejor desempeño. En cuanto al efecto en la reactividad por la densidad del refrigerante, en general se tiene un buen comportamiento, ya que en casi todos los casos estudiados se tiene un efecto en la reactividad negativo, o es positivo y pequeño. En las configuraciones con plutonio, en el caso de que se experimente una mayor fracción de vacíos en el refrigerante en la región del combustible, o sólo la región interna superior, entonces se obtiene un efecto positivo en la reactividad. Se obtiene un mucho mejor desempeño con configuraciones de combustible con ^{232}Th/^{233}U en su totalidad, ya que en todos los casos estudiados se tiene un efecto en la reactividad negativo, o un efecto positivo muy bajo. La distribución de potencia es similar en todas las configuraciones de combustible, teniendo un anillo con la mayor potencia en la región externa de combustible. Las configuraciones de combustible con ^{232}Th/^{233}U en su totalidad tienen la distribución de potencia más homogénea. Todas las configuraciones de combustible tienen una β_{eff} similar y muestran un buen margen de parada, ya que es más alto que el 1% dk/k al inicio del ciclo en todos los casos.

Contents

List of Figures

List of Tables

1. Introduction

In order to fulfill the future global energy demand with sustainable energy, nuclear power has to be taken into account, as it is a low carbon technology and has the capability to satisfy the global demand with low environmental impact [1].

Taking this into account, in 2002 six promising systems and their associated research and development needs were selected and described in the Generation IV International Forum. The Generation IV systems feature increased safety, improved economics for electricity production, hydrogen for transportation applications, reduced nuclear wastes for disposal, and increased proliferation resistance [2].

Most of the above mentioned reactors use UO_2 and MOX as fuel. Regarding the sustainability goal, it is necessary to have fuel alternatives that allow a better use of the resources in order to extend the nuclear energy life.

As thorium is three to four times more abundant than uranium over the Earth's Crust, it becomes an excellent candidate to be used as nuclear fuel. ^{232}Th would play a role equivalent to ^{238}U for use in a nuclear reactor, as both elements are fertile and can capture neutrons to transmute into a fissile isotope capable of sustaining a chain reaction [3]. A good option to carry out this process are fast reactors, since the high neutron flux facilitates the transmutation process [4].

For this work, the Advanced Sodium Technological Reactor for Industrial Demonstration (ASTRID) was selected. The ASTRID reactor uses a MOX based fuel, therefore, it is pretended to analyze the reactor behavior with the inclusion of thorium to take advantage of its breeding capability.

The main goal of this thesis is to study the ^{233}U breeding capability from the thorium utilization and to analyze the neutronic behavior of the ASTRID reactor under these conditions. Two thorium fueled strategies were analyzed, based on a reference fuel vector, composed with a mixture of U-Pu MOX fuel, which was modified as follows. For the first strategy, all uranium isotopes in the fertile zone were replaced for a mixture of ^{232}Th/^{233}U, leaving the fissile zone with its U-Pu MOX composition. For the second strategy, the fertile zone uses the composition of the first strategy, and all the uranium and plutonium isotopes in the fissile zone were replaced for a mixture of ^{232}Th/^{233}U. The MCNP6 code [5] with the ENDF/B-VII.0 cross section library [6] was used to perform the calculations.

The structure of this thesis is as follows: In Section 2 there is a short description of the advantages of the use of thorium as fuel. In Section 3 the MCNP code is briefly described. In Section 4 the ASTRID reactor and its features are described. In Section 5, the MCNP ASTRID model and the different fuel strategies are described. In Section 6 the results and comparisons of the different fuel configurations are presented. The conclusions are presented in Section 7.

2. Thorium

Thorium is a naturally occurring radioactive element with potential application in the nuclear fuel cycle. Thorium has no fissile isotopes, meaning that unlike uranium it cannot be enriched to produce a viable nuclear fuel. Natural thorium is entirely composed by the isotope ^{232}Th.

^{232}Th would play a role equivalent to ^{238}U for use in a nuclear reactor. Both elements are fertile and can capture a neutron to transmute into a fissile isotope capable of sustaining a chain reaction. In the case of ^{232}Th the fissile isotope produced is ^{233}U, which is an excellent fissile isotope in a fast spectrum, superior to ^{235}U and close to ^{239}Pu that are used today because of its high neutron yield per neutron absorbed (η factor). A self-sustained chain reaction requires less ^{233}U than ^{235}U. Both the thorium base material and ^{233}U have potential applications in the nuclear fuel cycle [7].

The average concentration of thorium in the Earth's crust is reported to be three to four times higher than the one of uranium. More relevant are the number and the significance of large scale and rich deposits [7].

Resources have been identified in several countries, amounting to a global total of roughly 4 to 6 million tons, with estimates varying somewhat due to differing methods used. Countries with significant thorium resources (>100 000 tons Th) include Turkey, Brazil, India, United States, Australia, Venezuela and Norway. Resources have also been documented in Canada, Greenland, the Russian Federation and South Africa [7].

Today, thorium is recovered mainly from the mineral monazite as a by-product of processing heavy-mineral sand deposits for titanium-, zirconium-, or tin-bearing minerals. Given its relative abundance and the current absence of a significant market, no specific efforts have been made in recent decades to improve the knowledge of thorium resources. Undoubtedly, the development of demand for thorium would lead to the identification of significant additional resources.

Thorium dioxide (ThO_2) has a melting point of 3370°C well above that of UO_2 (2840°C) and a slightly better thermal conductivity. Thorium dioxide is the highest oxidation state of thorium which means the material will not oxidize further while in long term storage.

The single dominant isotope of thorium does not fission when it absorbs a neutron at thermal energy. However ^{232}Th is a fertile isotope, transmuting to ^{233}U upon neutron absorption (Figure 2.1.).

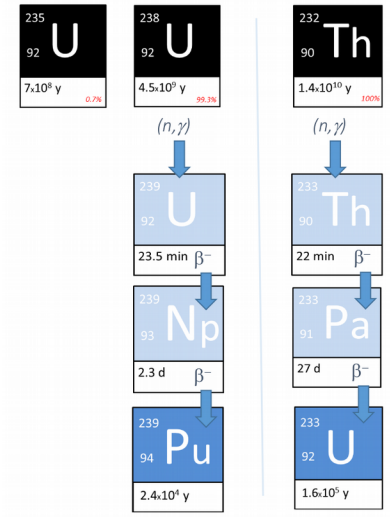

Figure 2.1. Thorium decay process [7]

2.1. Thorium in the Nuclear Fuel Cycle

Thorium fuel has been proposed for almost every type of reactor conceivable. The first ^{233}U reactor was built in 1961 to study advanced thorium reactor concept. The first commercial application of thorium-uranium fuel occurred in August 1962 at the Indian Point-1 Nuclear Power Plant. The first reactor fueled with fissile ^{233}U was the Oak Ridge National Laboratory molten-salt reactor in October 1968. Thorium and uranium fuel were efficient enough to demonstrate conceptual fissile fuel breeding with a water-cooled reactor at the Shippingport light water breeder test reactor from 1977 to 1982 [3].

The Thorex process requires a mixture of hydrofluoric and nitric acids in place of the second only for uranium and plutonium fuels. Therefore, the implementation of the Thorex process at industrial scale can only be envisaged in the medium term after demonstrations at pre-industrial scale have been made.

Technical and economic studies are needed to assess the commercial viability of using thorium in comparison with fuel cycles using uranium and plutonium. This commercial viability indeed depends on the price of uranium, on the breeding and conversion performances achievable in either type of reactor, on the cost of recycle of ^{233}U and plutonium (investment and operating cost for fuel reprocessing and re-fabrication), as well as on costs associated with the fuel cycle back-end. Non-proliferation issues also need to be thoroughly assessed.

Closed thorium-based fuel cycles however are very subject to proliferation risks as ^{233}U is a weapon grade material and its critical mass is only 1/3 of that of ^{235}U.

Recycled ^{233}U naturally benefits from some radiation protection as associated traces of ^{232}U decay into ^{228}Th, and a series of daughter products including ^{208}Tl and ^{212}Bi, that generate heat and high energy gamma rays (2.6 and 1.8 MeV respectively). It also benefits from some physical protection as manufacturing of ^{233}U-based fuels must be performed remotely in a shielded production line. In addition, these high energy gamma rays constitute an excellent radiative signature of reprocessed ^{233}U that makes its detection easier and its potential diversion more difficult.

However, the proliferation potential of thorium fuel cycles with less than 20% fissile materials (as recycled ^{233}U, ^{235}U or plutonium) is believed to be comparable with that of the uranium fuel cycle

with recycle of plutonium. Indeed, thorium fuel cycles require sizably higher uranium enrichment levels than uranium fuel cycles. Furthermore, separation work that is needed to produce pure ^{233}U from used U/Th or Pu/Th fuel may be judged comparable to that required to produce separated plutonium from the uranium/plutonium fuel cycle, even though the chemical reprocessing of used thorium-based fuels remains a technical challenge today.

For all above reasons, reaching an international agreement on banning the use of highly ^{233}U enriched uranium cannot be excluded [3].

3. The MCNP Monte Carlo Code

The MCNP code (Monte Carlo N-Particle) is developed by Los Alamos National Laboratory, and is one of the most used codes in reactor physics and considered as a reference. It is a general purpose particle transport code that uses the Monte Carlo numeric method for the solution of problems and can use different modes:

- Neutron, photon or electron transport
- Neutron/photon transport
- Neutron/photon/electron transport
- Photon/electron transport
- Electron/photon transport
- Criticality calculations for fissile systems, with the computation of the neutron multiplication factor keff

It has many applications. Nuclear safety, shielding calculations, detectors design and analysis, personal dosimetry, etc. The code uses continuous energy nuclear data library such as the ENDF (Evaluated Nuclear Data File) or the ENDL (Evaluated Nuclear Data Library) [8].

3.1. The Monte Carlo Method [9]

The solution of many problems in mathematics can be expressed in terms of an integration of a function. One is often interested in obtaining a numerical value from such expressions, but this is often difficult or tedious to obtain analytically. For integrals of the form

$$I = \int_{\Omega} f(x)\,dx$$

in which Ω is the domain of integration, the integral I can be related to an expectation of a random variable with respect to some probability measure. For probability measures of a random variable X that have a density ρ(x) the expectation can be expressed as:

$$E(f(X)) = \int_{\Omega} f(x)\rho(x)\,dx$$

The integral I can be expressed in terms of an expectation in a number of different ways. One rather general approach is to use a density having the feature that $\rho(x) > 0$ whenever $f(x) 6 \neq 0$. This gives that:

$$I = \int_{\Omega} f(x)\,dx = \int_{\Omega} \frac{f(x)}{\rho(x)}\rho(x)\,dx$$

$$I = E\left(\frac{f(X)}{\rho(X)}\right)$$

$$I = E(g(x))$$

where $g(x) = \frac{f(x)}{\rho(x)}$. In the case of a domain of integration Ω which is finite, we can always use the random variable X uniformly distributed on Ω with density $\rho(x) = \frac{1}{|\Omega|}$ to obtain:

$$I = \int_{\Omega} f(x)dx = \int_{\Omega} \frac{f(x)}{\frac{1}{|\Omega|}} \frac{1}{|\Omega|} dx$$

$$I = |\Omega| E(f(X))$$

The utility of expressing the integral in terms of an expectation derives from the *Law of Large Numbers*, which states that for a collection of independent identically distributed random variables $\{X_i\}_{i=1}^{\infty}$:

$$E(g(X)) = \lim_{N \to \infty} \frac{1}{N} \sum_{i=1}^{N} g(X_i)$$

This offers a way to estimate the numerical value of I, in particular:

- Generate N random variates $\{X_i\}_{i=1}^{N}$ with distribution ρ(x) on Ω.
- Approximate the expectation using the *Law of Large Numbers* $I \approx \frac{1}{N} \sum_{i=1}^{N} g(X_i)$

This gives a probabilistic approach to estimating the quantity I. This general class of methods are called *Monte Carlo Methods* and were proposed for statistical sampling in the 1940's by S. Ulam. The approach is nicknamed after a famous Monaco casino in the Mediterranean.

The Monte Carlo method has an accuracy which can be estimated as:

$$error = \left| \frac{1}{N} \sum_{i=1}^{N} g(X_i) - I \right|$$

$$error = \left| \frac{\sigma_g}{\sqrt{N}} \left(\frac{\sum_{i=1}^{N} g(X_i) - N I}{\sigma_g \sqrt{N}} \right) \right|$$

$$error \approx \left| \frac{\sigma_g}{\sqrt{N}} \eta(0,1) \right|$$

where

$$\sigma_g^2 = \int_{\Omega} (g(x) - I)^2 \rho(x) dx$$

and η(0, 1) denotes a standard normal random variable (Gaussian random variable) with mean zero and variance 1. The last approximation was obtained by using the *Central Limit Theorem*, which states that for a sum of i.i.d random variables Y_i with mean μ and finite variance σ^2:

$$\frac{\sum_{i=1}^{N} Y_i - N_{\mu}}{\sigma \sqrt{N}} \to \eta(0,1), as\ N \to \infty$$

This shows that asymptotically the error converges at a rate $O(\frac{1}{\sqrt{N}})$, independent of the dimensionality of the problem considered. Furthermore, the convergence rate in the Monte Carlo

method is strongly influenced by the prefactor σ_g which depends on the function f(x) and the sampling distribution with density ρ(x) that is used. The prefactor σ_g presents the primary avenue by which the convergence rate can be improved.

3.2. The Monte Carlo Method applied to the Transport Equation

[8]

The Monte Carlo method can be used to reproduce the history of a neutron in detail using a computer. Each stage of a neutron life depends on probability distribution functions. With this method it is possible to acquire the path of the neutrons through the medium, therefore obtaining the neutron distribution.

As the Monte Carlo method is a statistic based method, the result obtained is not unique, but an estimation with a confidence interval around the true value. Because of this, one of the disadvantages of the method is the great error obtained associated with the result. With the purpose of having an acceptable error magnitude, it is required to trace a large number of neutron histories, which considerably increases calculation time.

The neutron lifetime starts with its birth, either by an external neutron source or by fission, and ends with the absorption or escape from the system. The events occurring during the neutrons lifetime are registered and become the neutron history.

Suppose a neutron being originated at the point A in Figure 3.1. with known direction and energy. It will have a “free flight” until it has a collision with an atom in the medium, which can result in neutron absorption, finishing its history. In the case it is dispersed, the neutron has a change in energy and direction. These two changes are statistic processes, each having a probability distribution function. In Figure 3.1. it is shown that after the first dispersion, the same neutron has another “free flight” until it collides again, and so on.

To trace the neutron during its lifetime it is necessary to know its spatial coordinates, its direction in spherical coordinates and its energy. These variables are enough to define the state α of the neutron, where:

$$\alpha=\alpha(x,y,z;E;\theta,\phi)$$

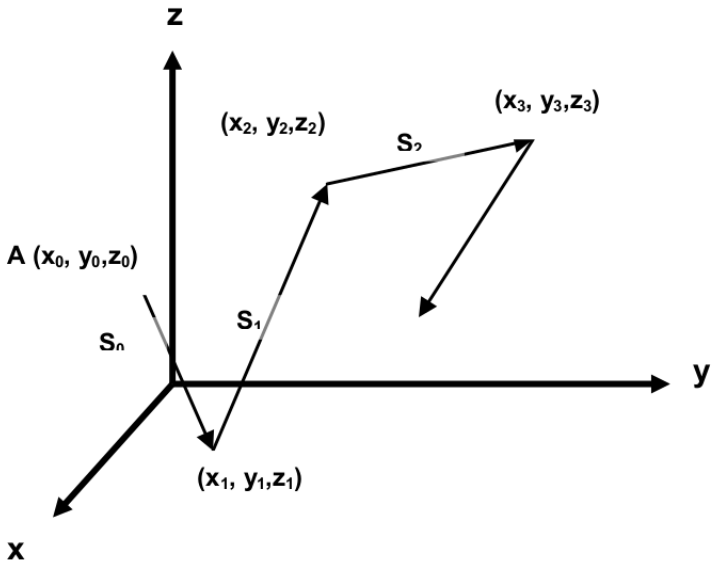

Figure 3.1. Random path of a particle through a medium [8]

A neutrons path can be built from collision to collision as a sequence of states α_0, α_1, … , α_n, where the "i" state is:

$$\alpha_i = \alpha_i(x_i, y_i, z_i; E_i; \theta_i, \phi_i)$$

Therefore, in the "i" state, a neutron has the spatial coordinates of the point where the collision happens, and the energy and direction of the neutron after that collision. Disregarding the beginning state, each state depends of the previous state and on the dispersion laws in the material of interest.

Math procedures are required to know the state of the next collision. If "s" is the longitude of the path that the neutron travels until its next collision, the probability of the neutron to travel the distance "s" without having an interaction is $e^{-\Sigma_t s}$. The probability of the neutron having an interaction in the interval ds is $\Sigma_t ds$, then the probability of the neutron having an interaction between s and s+ds is:

$$\Sigma_t e^{-\Sigma_t s} ds$$

Where Σ_t is the macroscopic total cross section. The next step is to select a random value for s using its probability function. Then the coordinates of the next collision will be:

$$x_{i+1} = x_i + s_i(sen\,\theta_i \cos\theta_i)$$
$$y_{i+1} = y_i + s_i(sen\,\theta_i\, sen\,\theta_i)$$
$$z_{i+1} = z_i + s_i(\cos\theta_i)$$

And the same goes to know the energy after the neutrons scattering.

The relation between the physic event and the random number is fundamental in this method, and it can be done by a probability function p(x), which describes the relative frequency of the random variable x comprehended in a determined interval.
We will define a probability density function as follows. Be $prob(x < X < x + \Delta x)$ the probability of the random variable in analysis to be within the interval (x, x+dx). This probability function is given by the expression:

$$prob(x < X < x + dx) = p(x)$$

Where p(x) is the probability of an interaction within the interval (x, x+dx) and if x occurs in an continuous interval:

$$prob(a < x < b) = \int_a^b p(x)\,dx$$

As a probability density function p(x) describes the relative frequency of the occurrence of x along the range of possible x values, then for all x:

$$0 \leq p(x)$$
$$\int_{-\infty}^{\infty} p(x)\,dx = 1$$

The function p(x) can be continuous or discrete. The energy spectrum of the fission neutrons χ(E) is a continuous probability density function. A materials absorption and scattering cross sections are discrete probability density functions.

3.3. Criticality Calculations [8]

In criticality calculations it is of great importance to estimate the value of the effective neutron multiplication factor keff. In this calculations, a group of neutron histories is referred as a keff cycle, or a neutron generation in reactor theory. The keff factor is given by the rate of the number of neutrons generated in fission events present in the cycle, divided by the number of neutrons whos histories are evaluated in this cycle (the number of neutrons at the beginning of the generation).

The expected value of the multiplication factor is estimated by averaging the events in the keff cycle. The expected value of the leak probability or the events that lead to capture can be obtained by the same way. The relative error in the keff estimation usually decreases as the as the number of keff cycles increase, therefore it is necessary a great number of cycles to obtain a good estimation. The multiplication factor is estimated through the following expression:

$$\bar{k} = \frac{1}{N} \sum_{i=1}^{N} k_i$$

where $\bar{k}$ is the multiplication factor estimated for the system of interest, end k_i es the multiplication factor estimated on the i-th cycle.

The Monte Carlo approximation can be summarized as follows: a sequence of random numbers r_i ($0 < r_i < 1$) is used to produce a random distribution of quantities that simulate the problem of interest. An example of how the Monte Carlo method works to obtain the neutron multiplication factor in a multiplicative medium is:

1. For the first cycle of the neutron multiplication factor (keff) calculation, establish the initial position of the neutron.
2. Use a random number to obtain the energy of the neutron.
3. Use the next random number to determine the cosine direction of the neutron.
4. Determine the location of the next collision with the next random number (with the distance traveled by the neutron depending on the materials cross section).

5. Verify the new neutron position to determine if it has escaped from the system: if this happens add a one to the total escapes an return to step 1 beginning another history or cycle; otherwise, continue.
6. Determine what kind of interaction happened in the new position based on the next random number. Each king of interaction has an associated a cross section that determines its probability of occurrence:
    - If the interaction is scattering, determine the energy of the scattered neutron using the next random number. Continue in step 3 to know the path of the scattered neutron.
    - If the interaction is capture, return to step 1 and start another cycle with a new neutron.
    - If the interaction is fission, determine how many neutrons are produced in this fission event (using the code libraries) and determine the total number of neutrons that has been produced in the cycle. Also determine the position of the produced neutrons in the fission to be used as the beginning of another cycle (replacing step 1 in future keff cycles)
7. When all requested histories are completed (enough for adequate statistic), evaluate keff by dividing the number of new neutrons created in this cycle by the number of histories evaluated in the cycle.

Repeat the process for as many cycles as it is required to obtain a proper statistic.

4. The ASTRID Advanced Sodium Technological Reactor for Industrial Demonstration

The ASTRID reactor is a Generation IV sodium cooled fast reactor, therefore some of its main characteristics are consumption of transuranics in a closed fuel cycle, enhanced utilization of uranium resources, and high level of safety achieved through inherent and passive means [10].

The first purpose of the ASTRID reactor is to demonstrate, at a sufficient scale, the following technological progress:

- Design of a high-performance core with improved safety, in particular, concerning prevention of severe accidents likely to cause complete core meltdown
- Improved resistance to severe accidents and external aggressions, in particular, design of redundant and diversified decay heat removal systems, as well as aspects related to the risk of recriticality and to molten core containment
- Search for an optimized and safe power conversion system intended to reduce or even completely remove the risk of interaction between sodium and water
- Reactor design options to make inspection and maintenance easier and, more generally, to improve the availability, the performance and the general economic characteristics of the facility

Therefore, ASTRID is a technological integration prototype which will make it possible to demonstrate the safety and the operation of 4th generation SFRs on an industrial scale. ASTRID will also be used as a test bench for the use of advanced inspection and repair techniques. Its size must be sufficient to allow extrapolation to commercial reactors, however, without being excessive to limit the cost and the industrial risk [11].

4.1. The SFR Sodium Cooled Fast Reactor [12]

The sodium-cooled fast reactor uses liquid sodium as the reactor coolant, allowing high power density with low coolant volume fraction. While the oxygen-free environment prevents corrosion, sodium reacts chemically with air and water and requires a sealed coolant system.

Plant size options under consideration range from small, 50 to 300 [MWe], modular reactors to larger plants up to 1500 [MWe]. The outlet temperature is 500-550°C for the options, which affords the use of the materials developed and proven in prior fast reactor programs.

The SFR closed fuel cycle enables regeneration of fissile fuel and facilitates management of minor actinides. However, this requires that recycle fuels be developed and qualified for use.

Important safety features of the Generation IV system include a long thermal response time, a reasonable margin to coolant boiling, a primary system that operates near atmospheric pressure, and an intermediate sodium system between the radioactive sodium in the primary system and the power conversion system. Water/steam and supercritical carbon dioxide are considered as working fluids for the power conversion system to achieve high performance in terms of thermal efficiency, safety and reliability.

With innovations to reduce capital cost, the SFR is aimed to be economically competitive in future electricity markets. In addition, the fast neutron spectrum greatly extends the uranium resources compared to thermal reactors and are more effective at fissioning transuranic actinides.

The SFR is an attractive energy source for nations that desire to make the best use of limited nuclear fuel resources and manage nuclear waste by closing the fuel cycle. The main characteristics of the SFR for actinide management mission are: consumption of transuranics in a closed fuel cycle, thus reducing the radiotoxicity and heat load which facilitates waste disposal and geologic isolation.

High level of safety achieved through inherent and passive means also allows accommodation of transients and bounding events with significant safety margins. The reactor unit can be arranged in a pool layout like the one depicted in Figure 4.1., or a compact loop layout. The SFR is considered to be the nearest-term deployable system for actinide management.

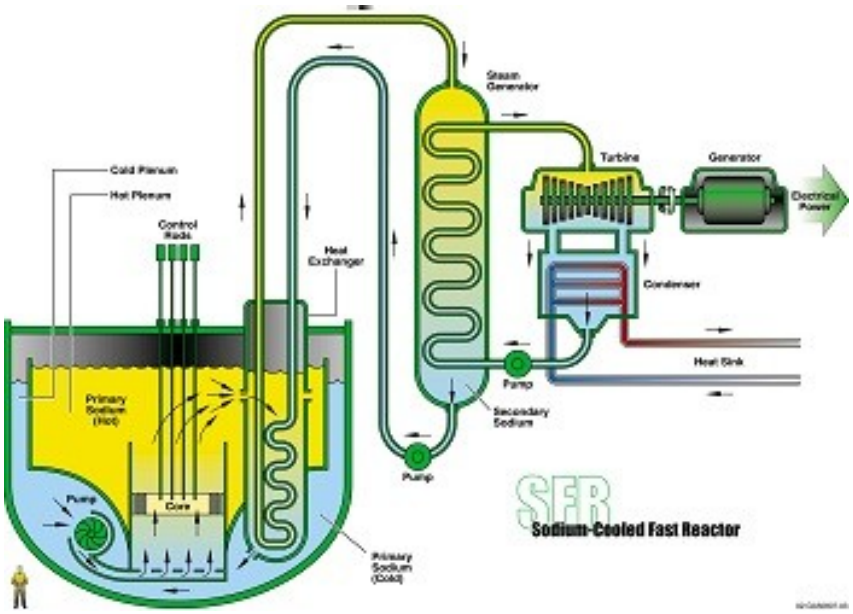

Figure 4.1. Pool type SFR [10]

4.2. The ASTRID Core

The reference fuel material is mixed oxide (U, Pu)O2. Significant experience feedback acquired for over more than forty years based on experimental and monitoring programmes carried out in Rapsodie, Phenix and Superphenix demonstrated that this fuel has an excellent behavior up to very high burn-up fractions.

For the first ASTRID cores, the cladding material of the fuel subassembly will be the 15-15 Ti work-hardened austenitic steel AIM1. This is the most advanced grade of this type of material. The use of this material will necessarily limit the burn-up fraction of the core. Switching to a ferritic or martensitic ODS type material grade will be performed gradually.

The fuel element is composed of a steel pin which contains the fuel in the form of pellets. A pin contains an axial heterogeneous fuel composed of UO2 fertile columns and (U, Pu)O2 fissile columns [11].

The core is composed of 291 hexagonal wrapped fuel Sub-Assemblies (S/As) grouped into two radial regions, which differ for both plutonium content and axial zoning. The inner zone is composed of 177 S/As (4 of them being diluent S/As with the same material composition as the fertile blanket) with a total active height of 1.1 [m] including a 0.2 thick internal axial blanket; in order to reduce power peaking, the latter is not foreseen in the outer region, which counts 114 S/As with a total active height of 1.2 [m]. A 30 [cm] thick axial blanket is incorporated below both the

inner and outer zone fissile fuel. Each S/As contains 217 pins in a triangular arrangement. In Figure 4.2. and Figure 4.3. it can be seen that it is a highly heterogeneous reactor.

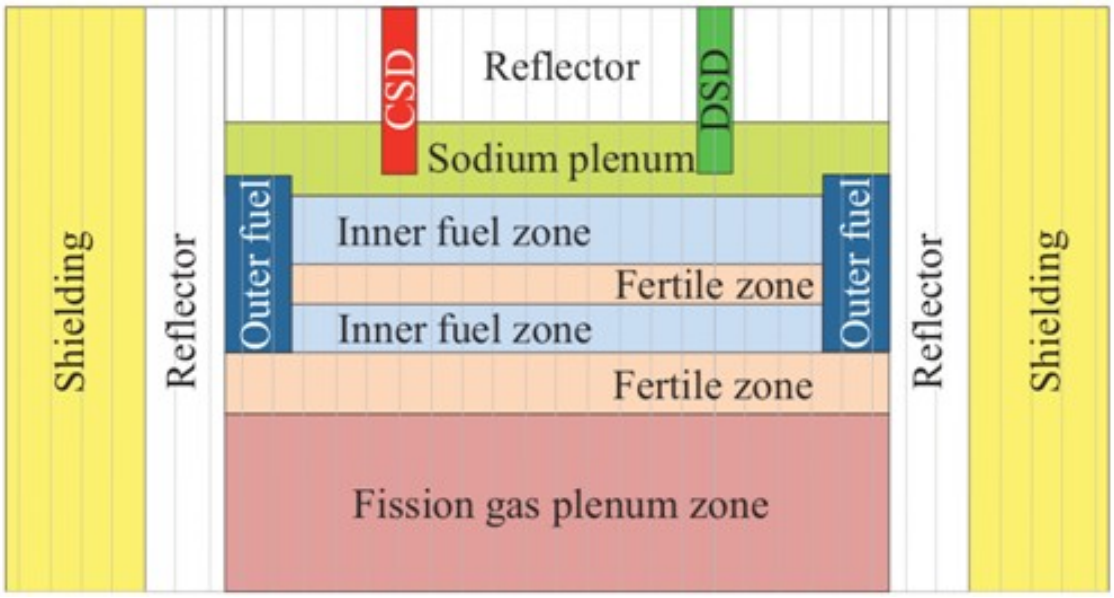

Figure 4.2. ASTRID core (lateral view) [13]

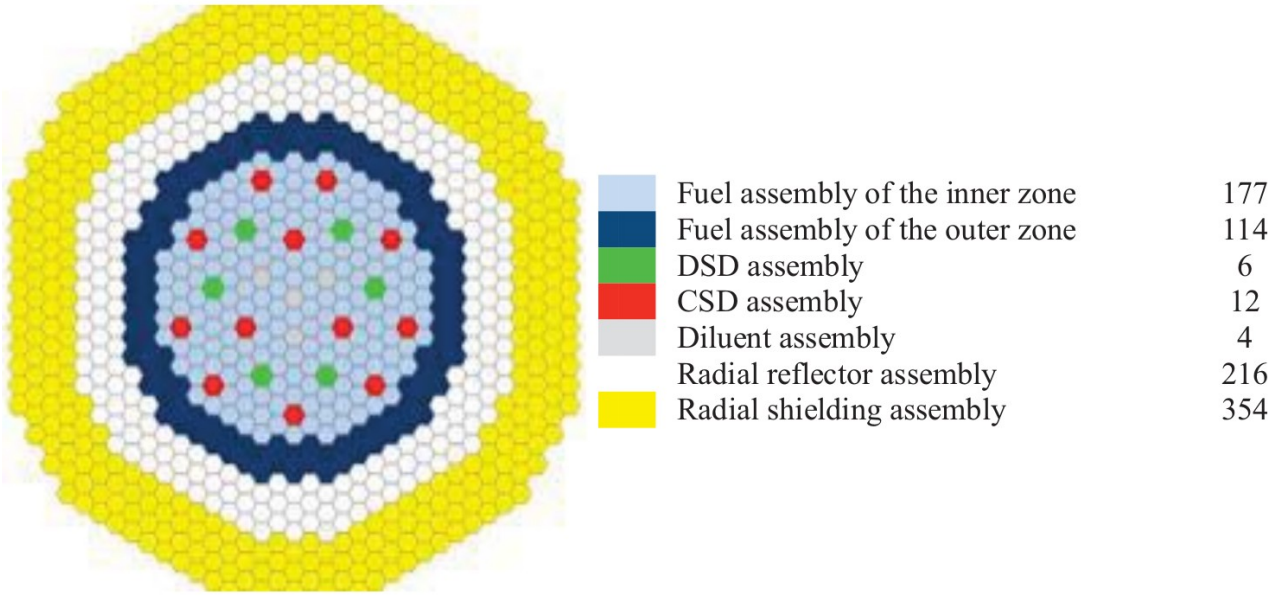

Figure 4.3. ASTRID core (upper view) [13]

Regulation, compensation and safety functions are handled by 12 control rods (CSDs) and 6 safety rods (DSDs), respectively, all located within the inner core region, as well as 4 diluent assemblies. Three rings of radial reflector assemblies and four rows of radial shielding assemblies surround the active core.

Based on the design specifications at room temperature, a thermal expansion template was first developed so as to provide a unified set of geometrical parameters and material compositions at operating conditions. This and the resulting reactor global parameters at nominal power are shown in Table 4.1. and Table 4.2.

Component	Temperature [°C]
Fuel (MOX @EoC fissile/UO2 @ EoC fertile)	1227 / 267
AIM cladding	475
Na coolant (average/inlet/outlet)	475 / 400 / 550
EM10 wrapper	475
316 Stainless steel diagrid	400

Table 4.1. ASTRID core operating temperatures [13]

Parameter	Value	Units
Nominal thermal power	1500	MW
Nominal mass flow rate	7752	$kg.s^{-1}$
Number of S/As – inner core	177	-
Number of S/As – outer core	114	-
Number of CSDs (nat and 48% enr. B_4C)	12	-
Number of DSDs (48% enr- B_4C)	6	-
S/A pitch	17.611	cm
Sodium inter-assembly gap thickness	0.473	cm
Inner fissile fuel height	60.456	cm
Outer fissile fuel height	90.685	cm
Internal axial blanket height	20.152	cm
Lower axial blanket height	30.228	cm
Sodium plenum height – inner core	39.555	cm
Sodium plenum height – outer core	29.479	cm

Table 4.2. ASTRID core global parameters at operating conditions [13]

The fuel composition is shown in Table 4.3.

Isotope / Fuel zone	Fissile zone	Fertile zone
^{235}U	0.0052	0.0022
^{238}U	0.7299	0.8792
^{238}Pu	0.0056	-
^{239}Pu	0.1043	-
^{240}Pu	0.0544	-
^{241}Pu	0.0214	-
^{242}Pu	0.0166	-
O / Zr	0.0622	0.1185

Table 4.3. Fuel composition (nuclide fraction) [14]

4.3. The ASTRID Nuclear Island

ASTRID follows the principle of “clean” primary system. The purpose of this principle is to prevent operation with burst open fuel clads. This prevents the contamination of the primary system with alpha emitters. The interest of this principle is to:

- Use the advantage of SFRs, as they have a very low dosimetry and release a smaller quantity of effluents and waste.
- Make maintenance, in-service inspection and repair operations easier.
- Make dismantling easier.

Fundamentally, the pool concept has intrinsic advantages which give it the potential to comply with the safety criteria (high thermal inertia, guarantee of the inventory in primary sodium). The experience feedback from the Fukushima accident reinforces this analysis even further: for safety reasons, the pool type primary system is therefore the system selected for ASTRID.

The power conversion fluid has a high pressure, and in case of leakage it may massively enter the primary system and generate a reactivity accident possibly combined with a chemical accident in the case of water-steam. If we don’t have an intermediate heat exchange system, the sodium-water reactions would occur with radioactive sodium and this would lead to a radiological hazard combined with a chemical risk. Therefore, an intermediate circuit with sodium as coolant will be used in ASTRID.

The internal architecture of the main vessel is an internal vessel with simple inner vessel with conical shape. It takes advantage of the studies carried out for Phenix, Superphenix and EFR. This architecture is the most mature and simplifies the design with respect to what was made on Superphenix.

The core neutron monitoring system is conventional and comprised of two systems of absorber rods:

- The control rods, used to control the core, compensate for the burn-up of the fuel and for normal reactor shutdown,
- The shutdown rods which only have a safety function, and which are used for reactor emergency shutdown.

These systems are redundant and diversified and they are frequently tested, in particular at each criticality of the reactor.

ASTRID has a core catcher located below the core. It is an important component to guarantee containment in case of complete core meltdown accident; it has sufficient dimensions to recover all the corium.

The decay heat removal is made by two families. The first family of DHR systems (DRC, for “Direct Reactor Cooling”) features an architecture which includes a Na/Na exchanger immersed in the main vessel, a Na/air exchanger and a final air cooling system. The second family (TMV, for “Through the main vessel”) is aimed at removing the residual heat through the vessel and providing diversification with respect to the systems which penetrate through the slab of the reactor. These systems can be controlled in all circumstances, like of loss of the electrical power supplies.

For the intermediate sodium loops there are 3 primary pumps, 4 intermediate exchangers and 4 secondary systems, each with a secondary pump. To improve natural convection in the secondary system, high-power electromagnetic pumps are being developed, expecting advantages with this type of technology in terms of reliability, maintainability and minimization of auxiliary systems [11].

5. The MCNP ASTRID Model

Using the above mentioned information, specially figures 4.2. and 4.3., and tables 4.1. and 4.2., the core was constructed in the MCNP6 code. The materials were selected in order to fulfill the description of its behavior in the oxide or metallic configuration and taken as reference. Then we used this reference cores to study its behavior in the afore mentioned experiments.

The process to build the model begins by defining the surfaces that will limit the fuel rods, the fuel assemblies, the different core regions and the core. These surfaces were used to define cells that will act as the core elements.

In MCNP6, a universe is a lattice or an arbitrary number of cells that, once defined, can be used to fill other cells within a geometry [15]. Different fuel rods were defined as universes to fill different fuel assembly lattices. These fuel assemblies were defined as universes to fill the reactor core. Figures 5.1., 5.2. show the fuel assemblies, and Figures 5.3. and 5.4. show the reactor core model.

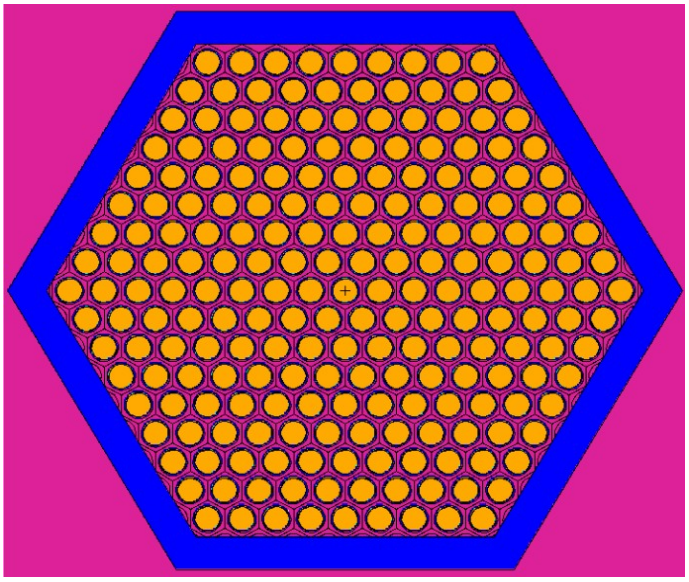

Figure 5.1. Fuel assembly universe (upper view) [5]

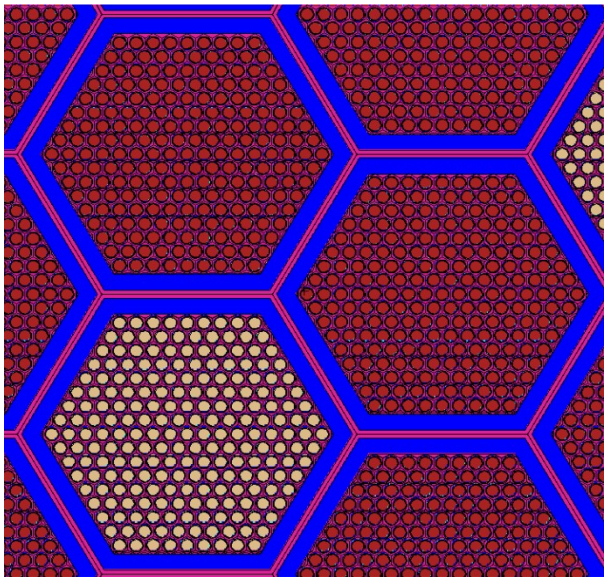

Figure 5.2. Core lattice section (upper view) [5]

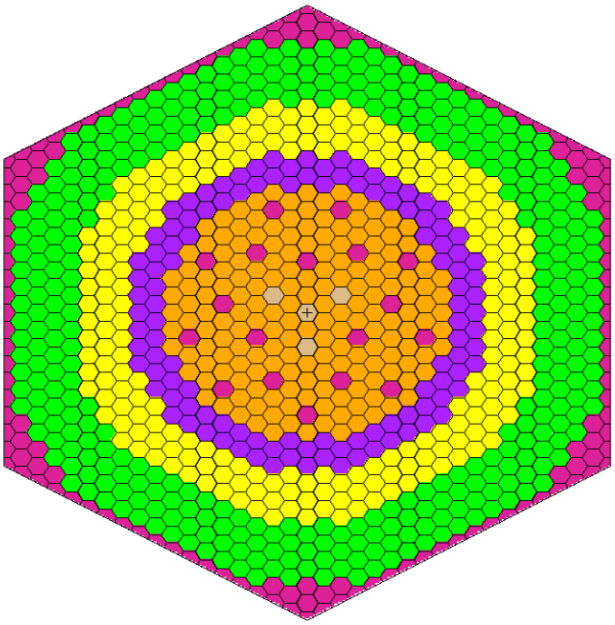

Figure 5.3. Reactor core (upper view) [5]

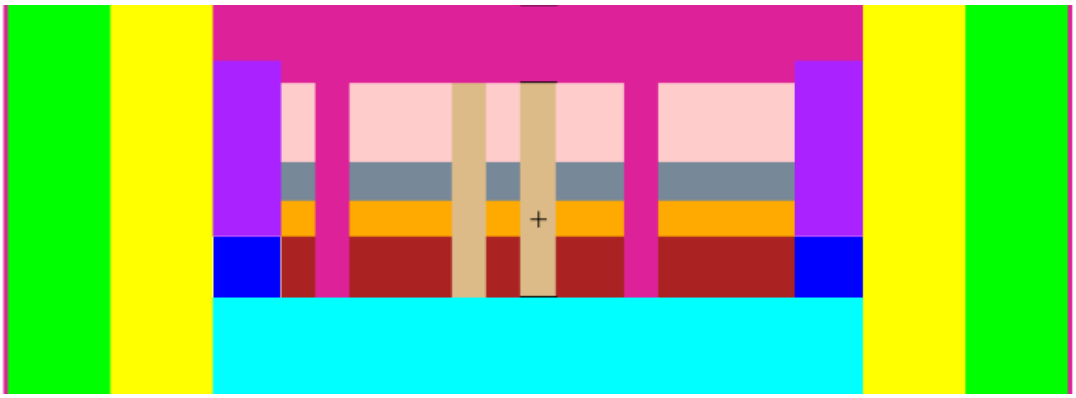

Figure 5.4. Reactor core (lateral view) [5]

5.1. Model Verification

For the calculations we used the MCNP6 code [5] with the ENDF/B-VII.0 cross section library [6], using 50000 neutrons per cycle, 30 discarded cycles and 200 active cycles. For the temperature we used 1200 [K] in the fissile fuel, 900 [K] in the fertile zone, and 600 [K] for the coolant and cladding.

The model was verified comparing the resulting keff in reference fuel at the EoC with the results from: "*European Benchmark on the ASTRID-like Low-void-effect Core Characterization: Neutronic Parameters and Safety Coefficients*" [13], which models the ASTRID reactor using different codes and libraries. In Table 5.1. we can prove that keff is among range.

Institution	keff
KIT	0.99966
PSI-E	1.00123
CEA	1.00432
GRS	1.00466
PSI-S	1.00431
HZDR-J	1.00394
HZDR-N	0.99796
UPM	1.00475
CIEMAT	1.00567
JRC	1.00218
UNAM	**1.00217**

Table 5.1. Core multiplication factors [13]

It was also verified comparing the results of the Doppler constants and the coolant void worth, as seen in Tables 5.2. and 5.3. respectively.

Institution	Fissile regions		Fertile regions	
	k_{D1}	k_{D2}	k_{D3}	k_{D4}
KIT	-623	-606	-314	-305
PSI-E	-684	-660	-321	-317
CEA	-661	-637	-327	-321
GRS	-576	-615	-278	-283
PSI-S	-661	-572	-335	-255
HZDR-J	-630	-594	-281	-311
HZDR-N	-583	-679	-285	-315
UPM	-584	-619	-273	-303
CIEMAT	-699	-592	-295	-234
JRC	-633	-612	-297	-333
UNAM	**-629**	**-730**	**-125**	**-202**

Table 5.2. Doppler constant [13]

Institution	k_{S1}	k_{S2}	k_{S7}	k_{S8}	k_{S9}
Benchmark average	-1450	450	-1700	1250	-450
UNAM	**-1494**	**600**	**1849**	**753**	**-1141**

Table 5.3. Reactivity effect of voiding [13]

Although there are differences, the main behavior is very similar. The values that move apart from the benchmark results need further investigation.

The radial power distribution was also used as a verification parameter. As in the Benchmark [13] the power distribution is difficult to compare directly, a more similar graphical representation was made to compare with our results. We can compare the power distribution main behavior seen in Figure 5.5.

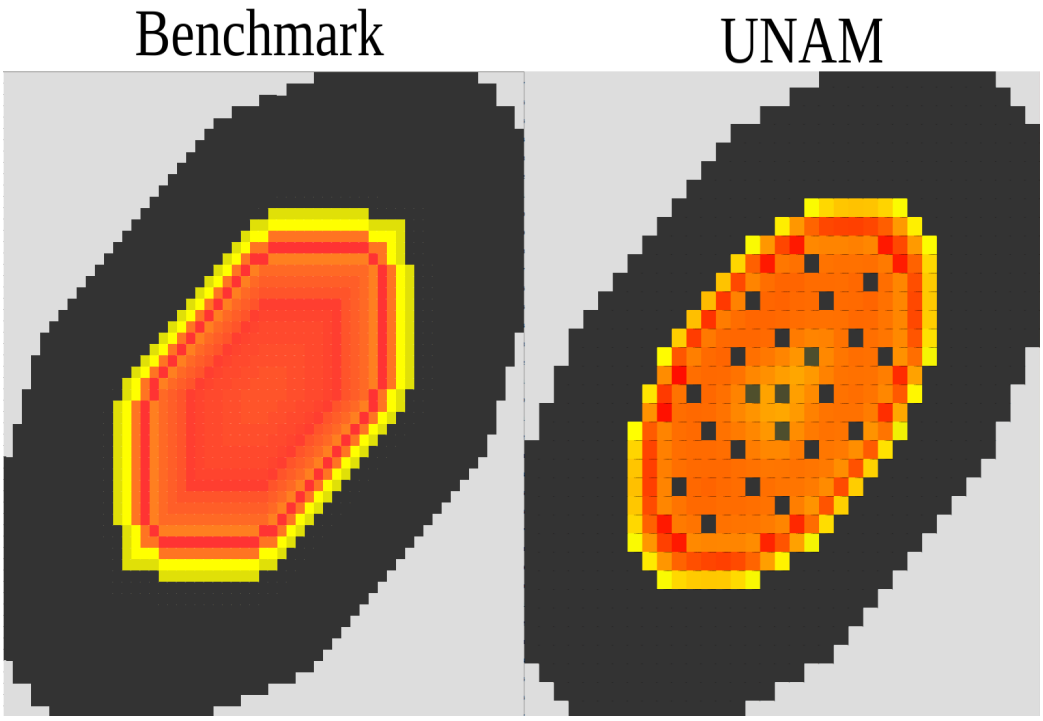

Figure 5.5. ASTRID reactor core radial power distribution [13]

The β_{eff} is the last parameter used to verify the model. Table 5.4. show the β_{eff} value from different codes and is consistent with the values obtained in this work.

Institution	β_{eff} [pcm]
KIT	358
PSI-E	366
CEA	356
GRS	N/A
PSI-S	347
HZDR-J	357
HZDR-N	344
UPM	N/A
CIEMAT	362
JRC	350
UNAM	**342**

Table 5.4. Delayed neutron fractions [13]

The model was also verified comparing the resulting keff in the reference fuel with the results from: "*A comparison between oxide and metallic ASTRID-like reactors*" [14], which models the ASTRID reactor in the MCNP code. In Figure 5.6. we can see the similitudes in the behavior of the keff along the operating cycle.

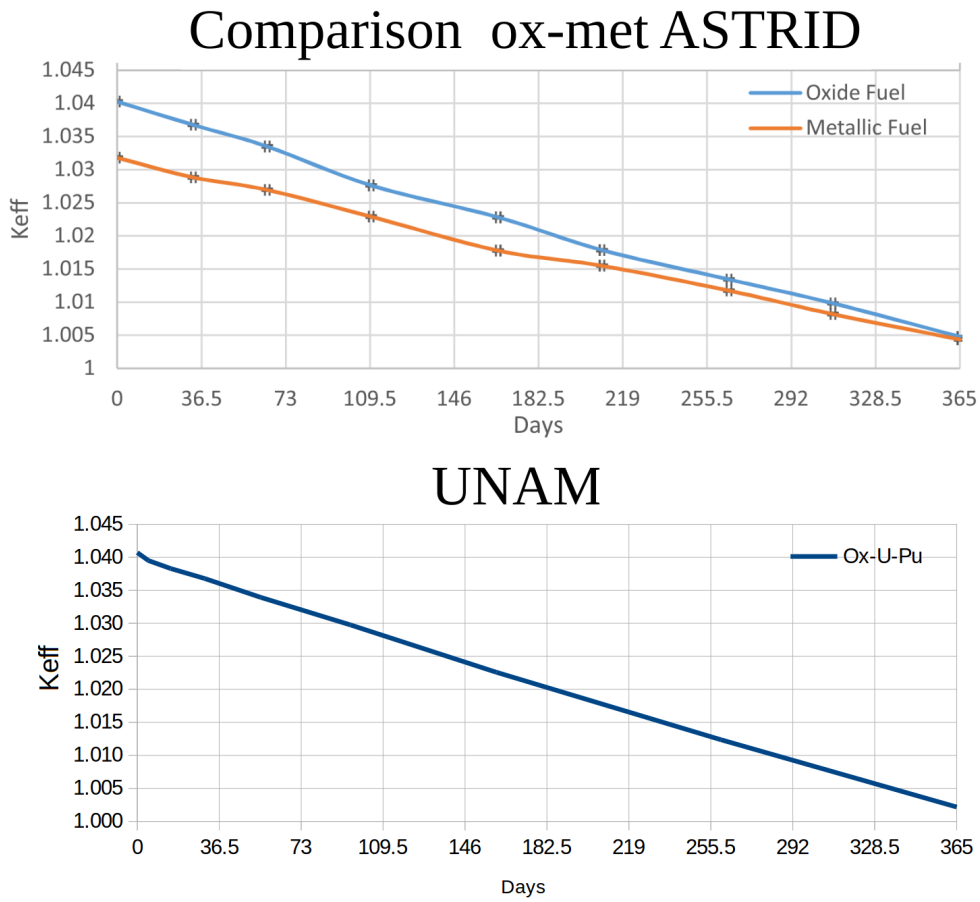

Figure 5.6. Keff comparison along operating cycle [14]

5.2. Thorium Based Fuel Strategies

Four strategies were defined to analyze the behavior of the reactor core with different type of thorium based fuel compositions.

5.2.1. Oxide Uranium-Plutonium-Thorium Core

In this analysis all uranium isotopes in the fertile zone of the reference oxide core were replaced for a mixture of oxide $^{232}Th/^{233}U$, leaving the fissile zone with its U-Pu MOX composition. As the fertile zone fuel was replaced, there was a reactivity loss. To solve this, ^{233}U was added to the fertile zone to provide positive reactivity to the core. The $^{232}Th/^{233}U$ ratio was fixed in order to have the keff at the BoC such that at the EoC keff was similar to that of the reference oxide core. In Table 5.1 the $^{232}Th/^{233}U$ fertile fuel vector is shown. Only the fuel composition was changed in this study, keeping the reference geometry and dimensions of the fuel assemblies and the reactor core unchanged.

Isotope	Weight percent (%)
^{16}O	12.1204
^{232}Th	86.3793
^{233}U	1.5003

Table 5.5. Ox-U-Pu-Th fertile fuel vector

5.2.2. Oxide Uranium-Thorium Core

In this analysis all uranium and plutonium isotopes in the fissile zone were replaced for a mixture of oxide $^{232}Th/^{233}U$, and using the $^{232}Th/^{233}U$ fuel composition of the previous section for the fertile zone. As the fissile zone fuel was replaced, there was a reactivity gain. To solve this, the ^{233}U concentration was adjusted to obtain the required keff using the same criteria as in the previous section. In Table 5.2 the $^{232}Th/^{233}U$ fissile fuel vector is shown. Again, only fuel composition was changed in this study, keeping the reference geometry and dimensions of the fuel assemblies and the reactor core unchanged.

Isotope	Weight percent (%)
^{16}O	12.1129
^{232}Th	71.9851
^{233}U	15.9020

Table 5.6. Ox-U-Th fissile fuel vector

5.2.3. Metallic Uranium-Plutonium-Thorium Core

In this analysis all uranium isotopes in the fertile zone of the reference metallic core were replaced for a mixture of metallic $^{232}Th/^{233}U$, leaving the fissile zone with its U-Pu-Zr metallic alloy. As the fertile zone fuel was replaced, there was a reactivity loss. To solve this, ^{233}U was added to the fertile zone to provide positive reactivity to the core. The $^{232}Th/^{233}U$ ratio was fixed in order to have the keff at the BoC such that the keff at the EoC is similar to that of the reference metallic core. In Table 5.3 the $^{232}Th/^{233}U$ fertile fuel vector is shown. Again, only fuel composition was changed in this study, keeping the reference geometry and dimensions of the fuel assemblies and the reactor core unchanged.

Isotope	Weight percent (%)
^{90}Zr	10.0000
^{232}Th	89.7740
^{233}U	0.2260

Table 5.7. Met-U-Pu-Th fertile fuel vector

5.2.4. Metallic Uranium-Thorium Core

In this analysis all uranium and plutonium isotopes in the fissile zone were replaced for a mixture of metallic $^{232}Th/^{233}U$, and using the $^{232}Th/^{233}U$ fuel composition of the previous section for the fertile

zone. As the fissile zone fuel was replaced, there was a reactivity gain. To solve this, the ^{233}U concentration was adjusted to obtain the required keff using the same criteria as in the previous section. In Table 5.4 the $^{232}Th/^{233}U$ fissile fuel vector is shown. Again, only fuel composition was changed in this study, keeping the reference geometry and dimensions of the fuel assemblies and the reactor core unchanged.

Isotope	Weight percent (%)
^{90}Zr	10.0000
^{232}Th	72.5696
^{233}U	17.4304

Table 5.8. Met-U-Th fissile fuel vector

5.3. Doppler Constants and Reactivity Effect of Coolant Density

In order to calculate the Doppler constant, the keff neutron multiplication factor was obtained at four different fuel temperature scenarios. First, we change the nominal 1200 [K] fissile zone temperature to 2500 [K] (D1), and from 1200 [K] to 900 [K] (D2), leaving the fertile zone temperature unchanged. Then we change the nominal 900 [K] fertile zone temperature to 1200 [K] (D3), and from 900 [K] to 600 [K] (D4), leaving the fissile zone temperature unchanged. The formula used to calculate the Doppler constant is:

$$K_D = - \frac{\rho(T_2) - \rho(T_1)}{\ln\left(\frac{T_2}{T_1}\right)}$$

To obtain the reactivity effect of coolant density, the keff neutron multiplication factor was obtained at eighteen different coolant density scenarios [13]. First, we decrease the coolant density to 70% of its nominal density, and then we increase the coolant density to 130% of its nominal density, and finally we averaged the values obtained for each one of the nine Sx zones shown in Figure 5.6, in which light violet indicates voiding of sodium plenum zones, amber indicates voiding of fuel zones, and pale blue indicates total voiding.

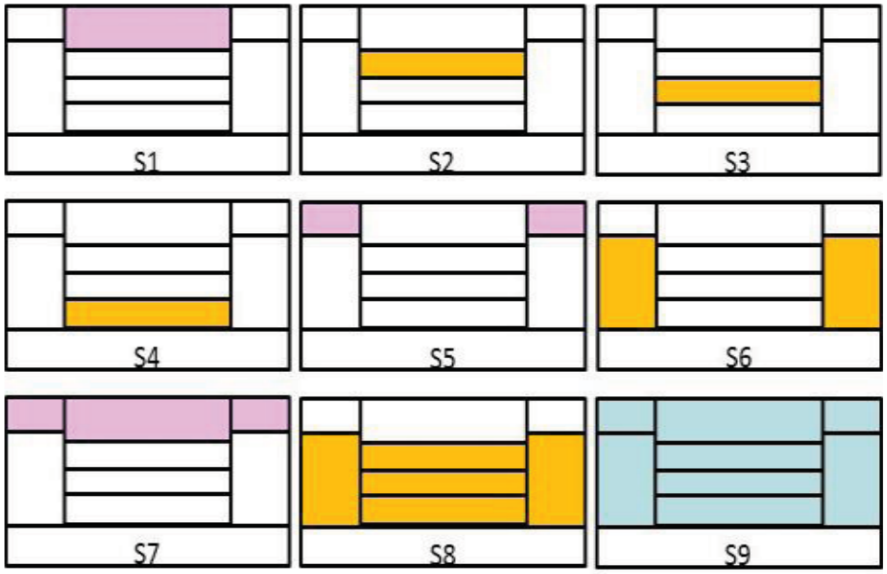

Figure 5.7. Schematic representation of the core voiding scenarios [13]

5.4. Shutdown Margin

To calculate the shutdown margin (SDM), the reactor core was set to the cold zero power condition and every control rod was fully inserted, except for that with the highest integral worth (any one of the tree red CSD nearest to the center of the reactor core, as seen in Figure 4.3.), then the keff was obtained. The SDM was calculated only at the BoC.

There are three different control rod positions available with the center of the reactor as reference because it is symmetric. To know the rod with the highest integral worth the keff was obtained fully inserting a control rod in these three different positions. The position that caused the highest negative reactivity was considered as the rod with the highest integral worth.

6. Results and Discussions

The keff value was obtained with MCNP6 for 365 days of operating cycle with 50000 neutrons per cycle, 30 discarded cycles and 200 active cycles, which lead to an estimated standard deviation of 17 pcm. This number of neutron histories were also used for the Doppler and the coolant density effect calculations at the BoC, for both (^{232}Th/^{233}U fertile and fissile) fuel designs.

We will be referring to the different core configurations as:
Ox-U-Pu → Reference oxide fuel core
Ox-U-Pu-Th → Oxide fuel core with ^{232}Th/^{233}U fertile fuel
Ox-U-Th → Oxide fuel core with ^{232}Th/^{233}U fertile and fissile fuel
Met-U-Pu → Reference metal fuel core
Met-U-Pu-Th → Metal fuel core with ^{232}Th/^{233}U fertile fuel
Met-U-Th → Metal fuel core with ^{232}Th/^{233}U fertile and fissile fuel

6.1. Energy Spectrum

Figure 6.1. and Figure 6.2. shows the neutron energy spectrum of the six mentioned fuel configurations.

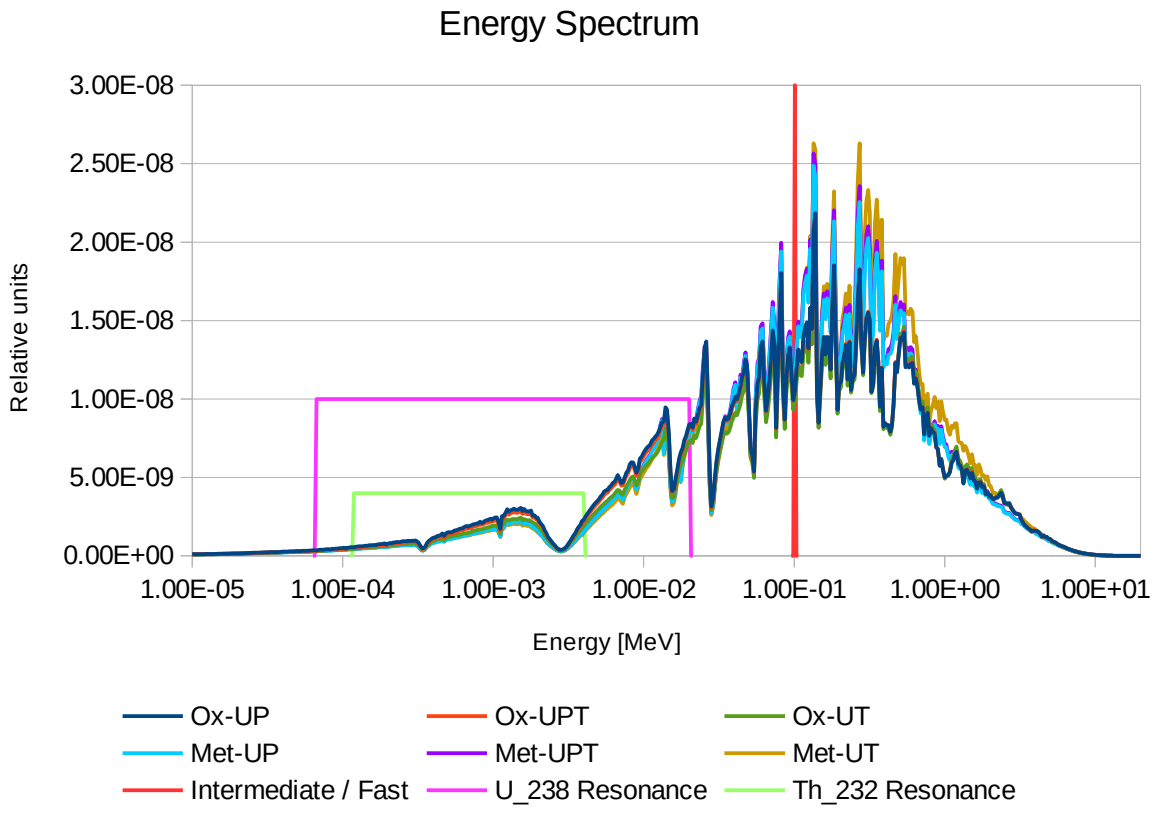

Figure 6.1. Neutron energy spectrum

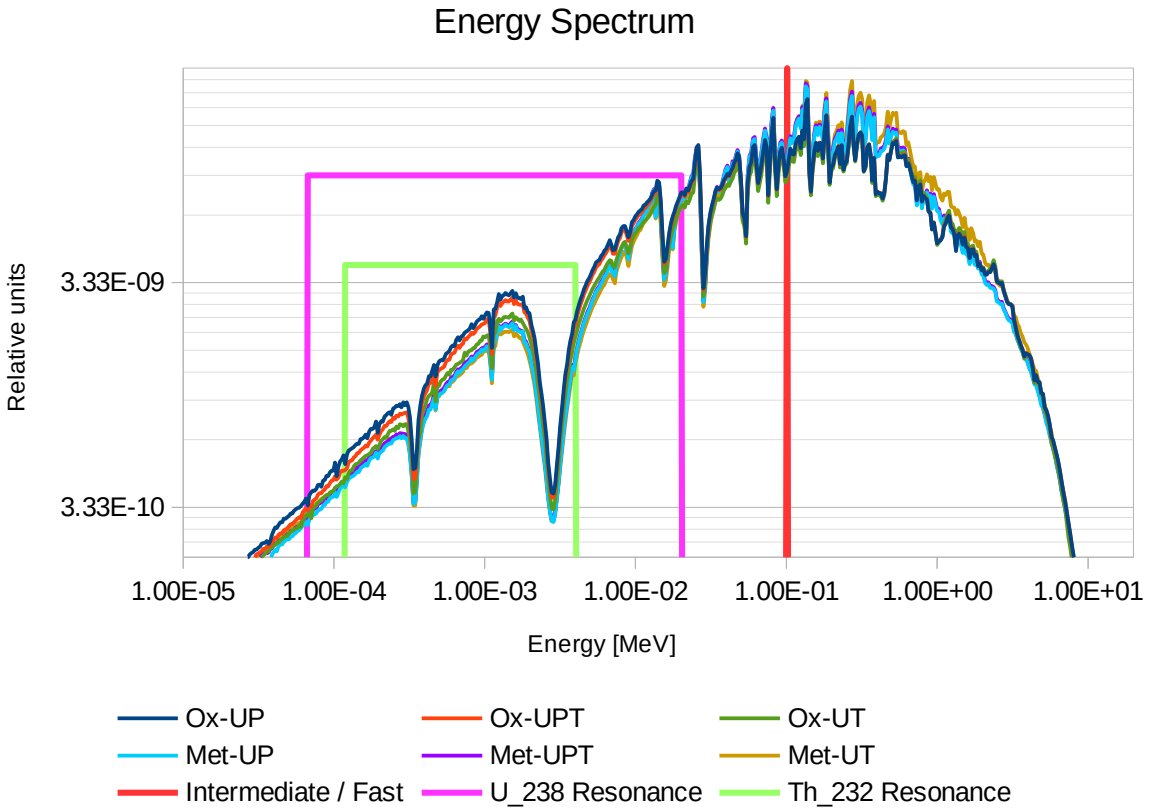

Figure 6.2. Neutron energy spectrum (Logarithmic)

In these Figures we can see that the oxide fuels tend to be in a bit lower spectrum, while metallic fuels tend to be in a harder spectrum. Besides that, the two fuels configuration with the full ^{232}Th/^{233}U fuel tend to be in a harder spectrum than the configurations with U and Pu.

As it can be seen in figures 6.1 and 6.2, the ^{232}Th resonances energy range is smaller than the ^{238}U resonances energy range, it is easier in this reactor to breed with U than with Th. Also, as the full ^{232}Th/^{233}U fuel has harder neutron energy spectrum, then neutrons will move away from the resonance making it even more difficult to breed with Th. This could be changed adding some local moderation to make breeding Th easier.

6.2. The keff Behavior

Figure 6.3. shows the keff evolution along the operating cycle of the six mentioned fuel configurations.

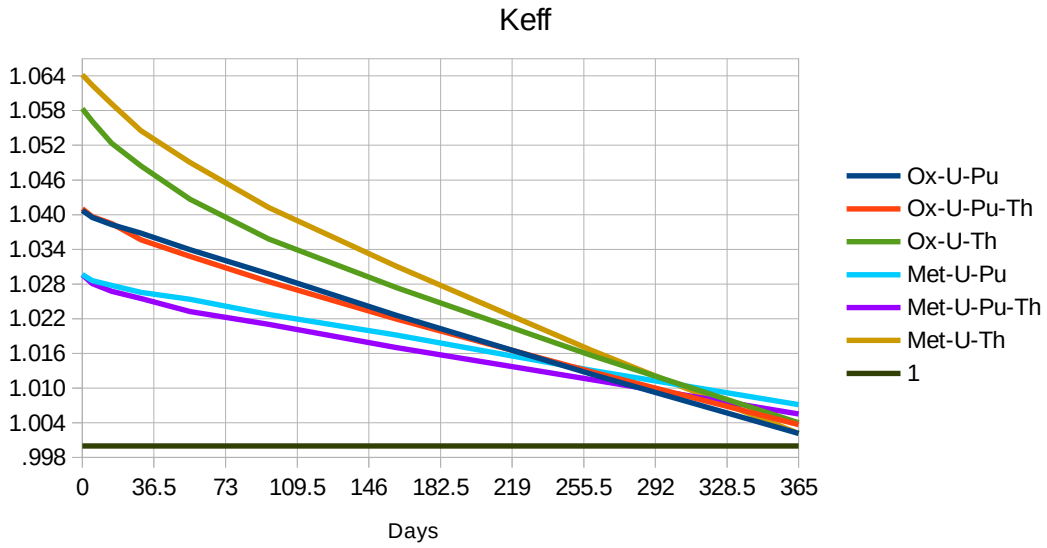

Figure 6.3. Keff behavior along the operating cycle

As can be seen, the keff in the Ox-U-Pu core and the Ox-U-Pu-Th core is very similar, although the keff in the Ox-U-Pu-Th core decreases faster for about the first 70 days, and then it decreases at a slower ratio than the U-Pu core, getting a slightly higher keff at the EoC.

On the other hand, the Ox-U-Th core needs a higher keff at the BoC to guarantee keff>1 at the EoC because the keff experience a strong decrease for about the first 70 days, then it decreases at a slower ratio, but it is still higher than the decreasing of the other two oxide fuel core configurations.

In the case of the Met-U-Pu core the keff has a smooth behavior, although the keff is not needed to be as high as the one of the Ox-U-Pu core at the BoC. This is because the metallic fuel has a higher density than the oxide fuel, and meaning a higher atomic density of fissile fuel, and will lose a lower fraction of fissile material with the burn up, which is also true for the Met-U-Pu-Th core fuel configuration.

For the Met-U-Pu-Th core the keff behavior is similar to the Met-U-Pu core, with the difference that the keff in the Met-U-Pu-Th core decreases faster for about the first 70 days, then it behaves almost the same way as the Met-U-Pu core.

Nevertheless, the Met-U-Th core needs the highest keff at the BoC to guarantee keff>1 at the EoC because the keff experience a very strong decrease for about the first 70 days, then it decreases at a slower ratio, but it is still higher than the decreases of all the other fuel core configurations.

For the two full ^{232}Th/^{233}U cases, a high keff is needed at the BoC to remain supercritical at the EoC. This is because they have a harder neutron energy spectrum, moving from the ^{232}Th resonance energy, causing more burn than breed than the other fuel configurations, and causing a higher keff decrease along the operating cycle. Also, as we have no Pu, there is no contribution of its isotopes in the neutronic behavior of the core.

The reduction in keff in the first 70 days, in all the four Th cases, is because the ^{233}Pa acts as a neutron poison due to its high capture cross section, compared to the fertile isotope ^{232}Th. Although the ^{233}Pa has a half-life of 27 days, it takes about 75 days to reach the equilibrium.

6.3. Main Isotopes Evolution

6.3.1. ^{233}U

Figure 6.4. and 6.5. shows the ^{233}U evolution along the operating cycle.

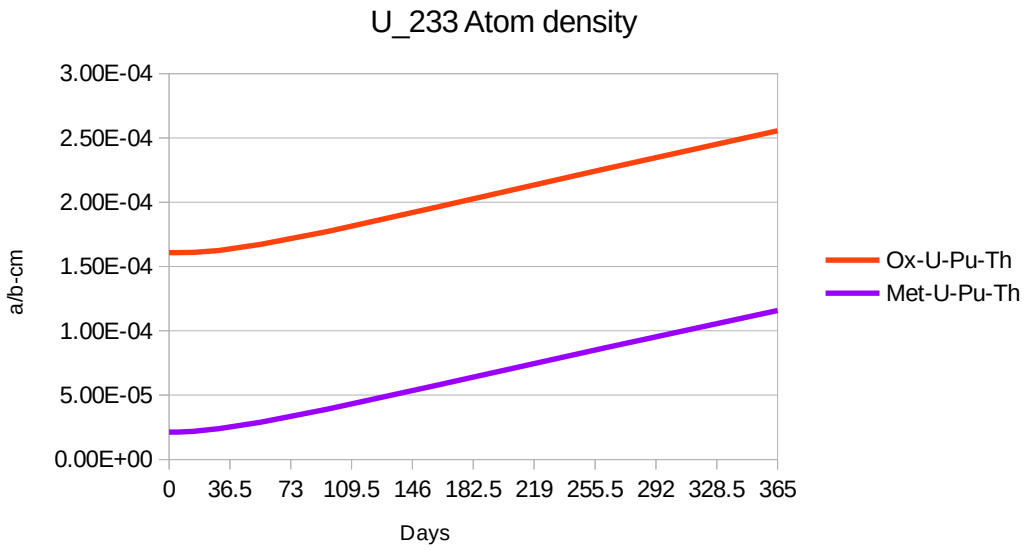

Figure 6.4. ^{233}U evolution along the operating cycle (Th in fertile zone)

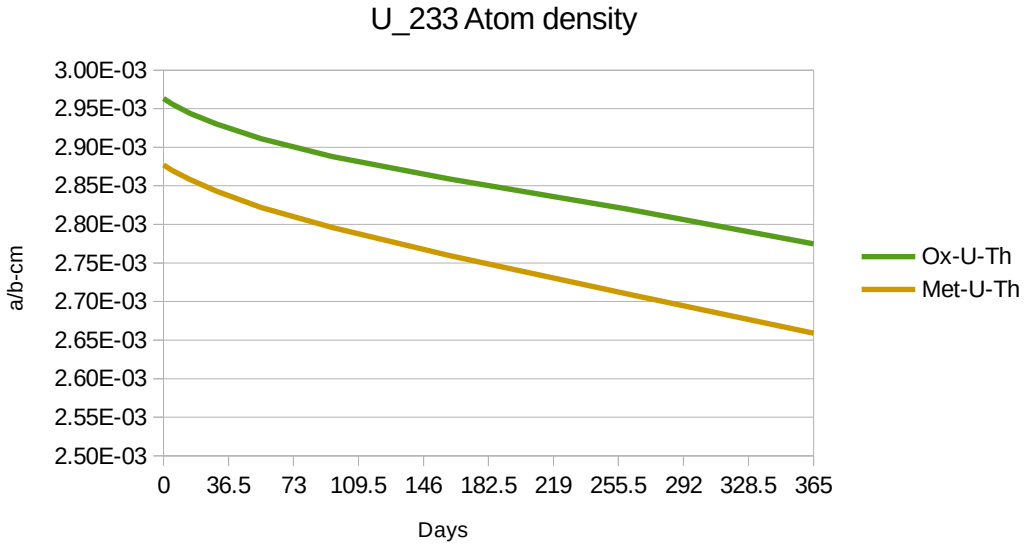

Figure 6.5. ^{233}U evolution along the operating cycle (Th in whole core)

As it can be seen, in the Ox-U-Pu-Th and the Met-U-Pu-Th cores, the ^{233}U is bred as expected, while it is mostly burning the ^{239}Pu. On the other hand, the full $^{232}Th/^{233}U$ fuel configuration does not breed more ^{233}U than it consumes. ^{233}U is absent in the other two fuel configurations.

6.3.2. ^{235}U

Figure 6.6. shows the ^{235}U evolution along the operating cycle.

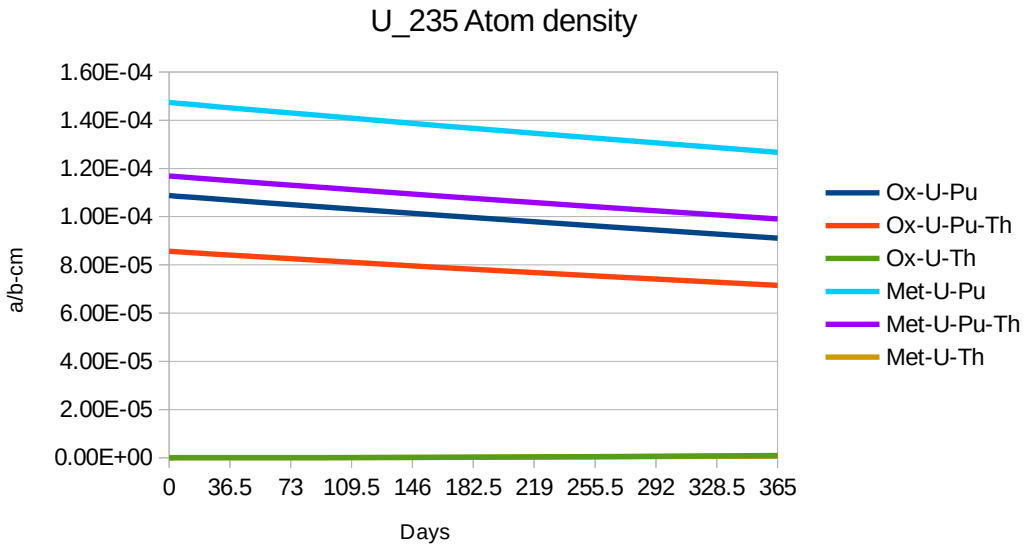

Figure 6.6. ^{235}U evolution along the operating cycle

As it is shown, all fuel configurations that contain natural uranium (containing low ^{235}U) burn it slightly along the cycle. It is absent in the other two full $^{232}Th/^{233}U$ fuel configurations.

6.3.3. ^{239}Pu

Figure 6.7. shows the ^{239}Pu evolution along the operating cycle.

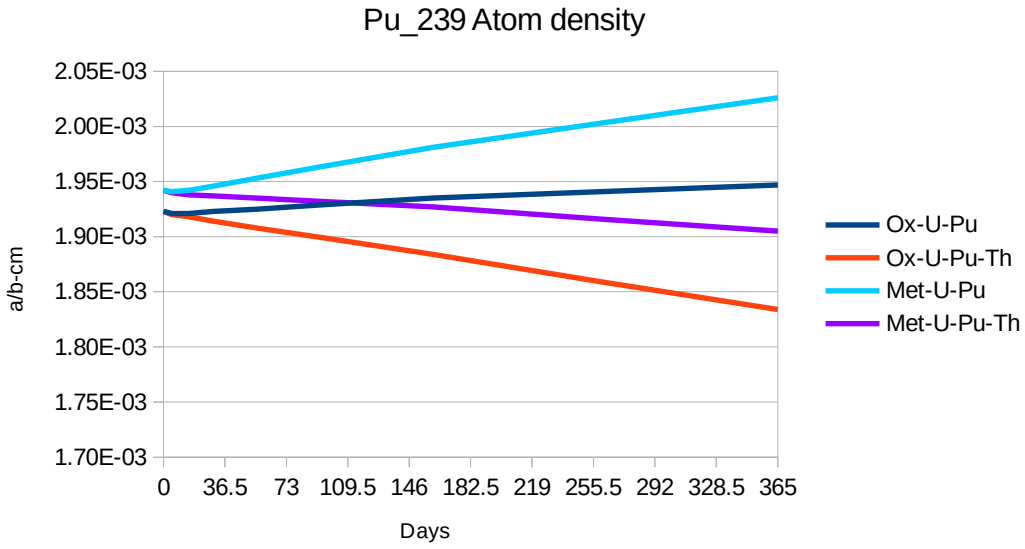

Figure 6.7. ^{239}Pu evolution along the operating cycle

As in the case of the ^{233}U, The Ox-U-Pu and the Met-U-Pu core fuel configurations breed ^{239}Pu from the ^{238}U in the fertile zone. While the Ox-U-Pu-T and the Met-U-Pu-Th core fuel configurations do not breed ^{239}Pu, as they breed ^{233}U instead.

6.3.4. ^{241}Pu

Figure 6.8. shows the ^{241}Pu evolution along the operating cycle.

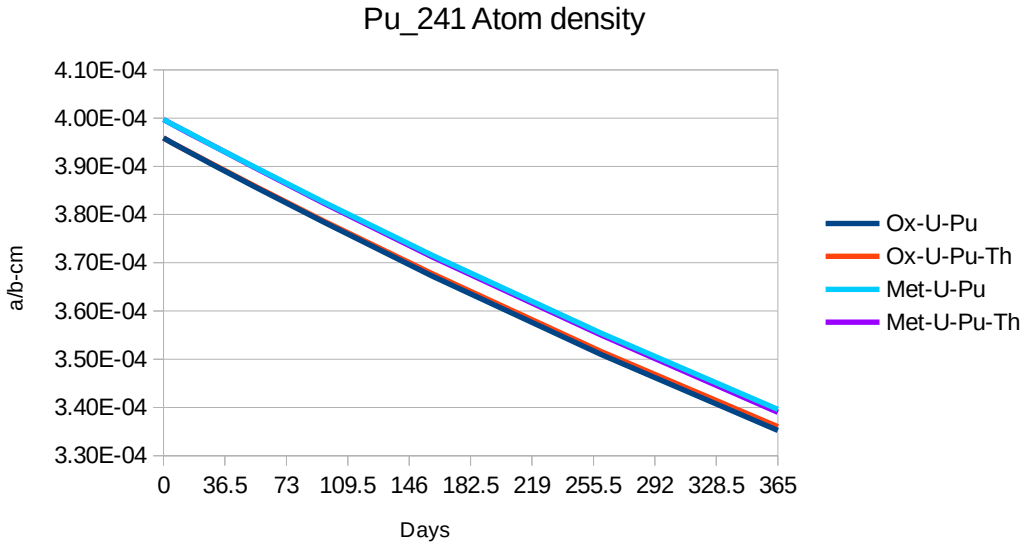

Figure 6.8. ^{241}Pu evolution along the operating cycle

The behavior of ^{241}Pu is alike in all configurations containing it. As we are in a hard spectrum reactor, it will (more likely) fission, or transmute by neutron capture, and no more of this isotope is accumulated along the operating cycle.

6.3.5. Am and Cm

Figure 6.9. shows the Am isotopes evolution along the operating cycle.

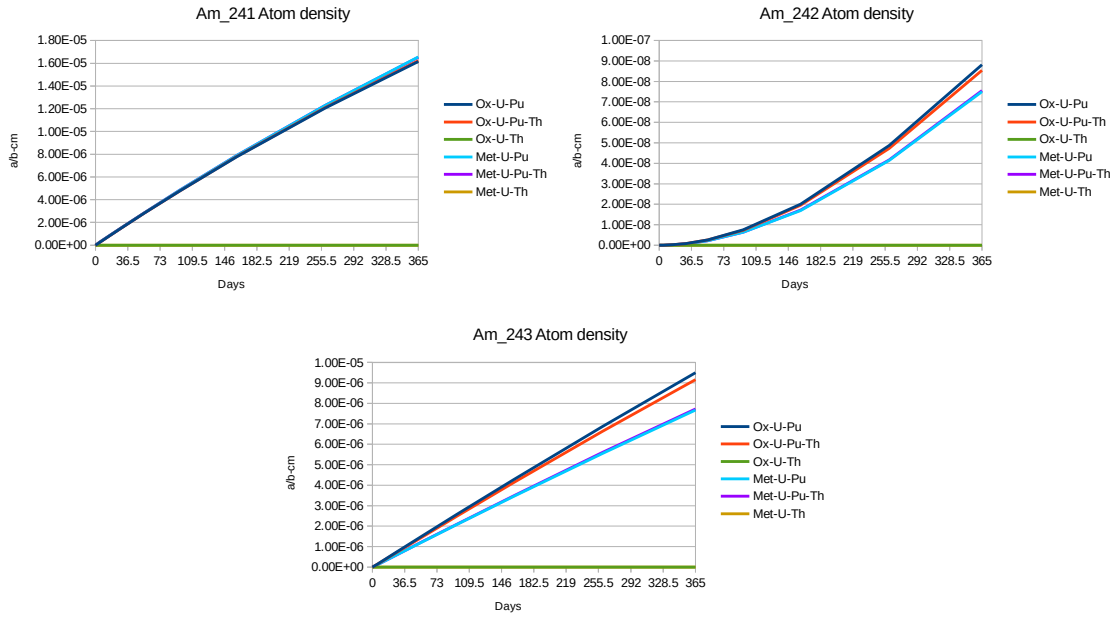

Figure 6.9. Am isotopes evolution along the operating cycle

Figure 6.10. shows the Cm isotopes evolution along the operating cycle.

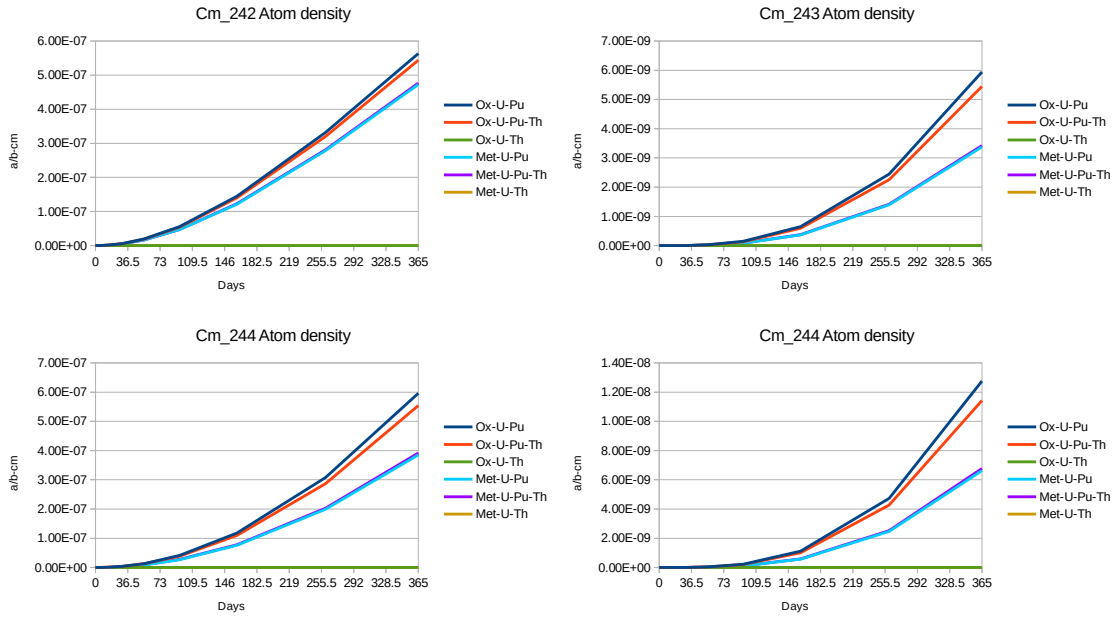

Figure 6.10. Cm isotopes evolution along the operating cycle

For both Am and Cm isotopes we have a similar behavior. Oxide fuels have the higher production of Am and Cm isotopes, remarking that the one with Th in the fertile zone has a lower production. Metallic fuels have lower production of the Am and Cm isotopes, and the one with Th in the fertile zone and the reference core have almost the same behavior. In the case of full $^{232}Th/^{233}U$ fuel, the Am and Cm isotopes are completely absent.

This is because the lower the atomic number of the element is, the harder it gets to produce heavier isotopes, thus making $^{232}Th/^{233}U$ fuel a good option to face the radiotoxic inventory issue.

6.4. Doppler Constant

Figures 6.11. and 6.12 shows the change on the keff value because of the change in the fuel temperature for the different fuel configurations and temperature zones. Figure 6.11. for the fissile fuel zone and 6.12. for the fertile fuel zone.

As expected, when the temperature increases, the keff value decreases. The same for the case in which the temperature decreases, the keff increases. Both have a similar behavior, noticing that the keff value is more sensitive to the change of temperature in the fissile zone.

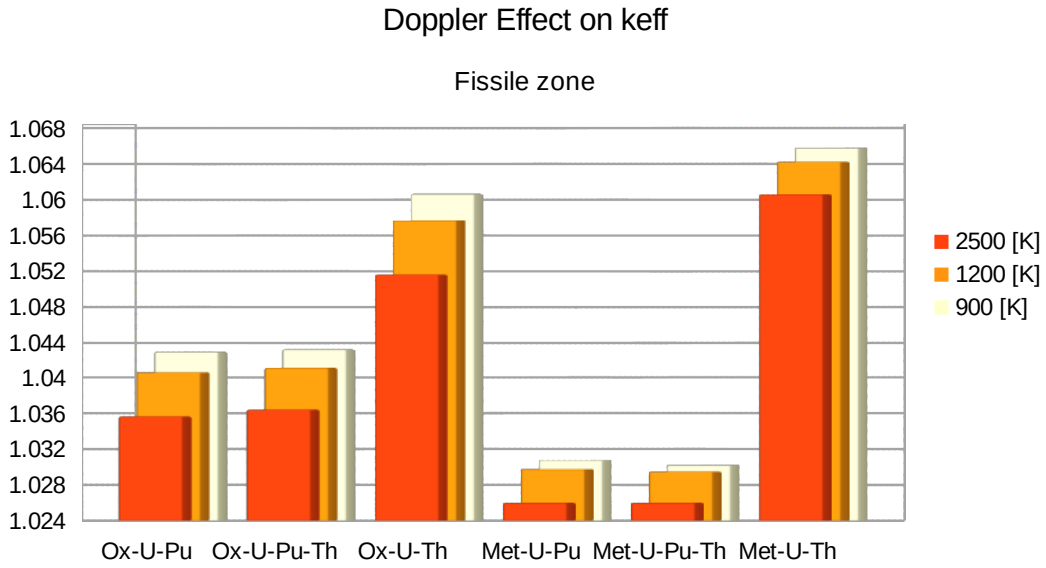

Figure 6.11. Doppler effect on keff (fissile)

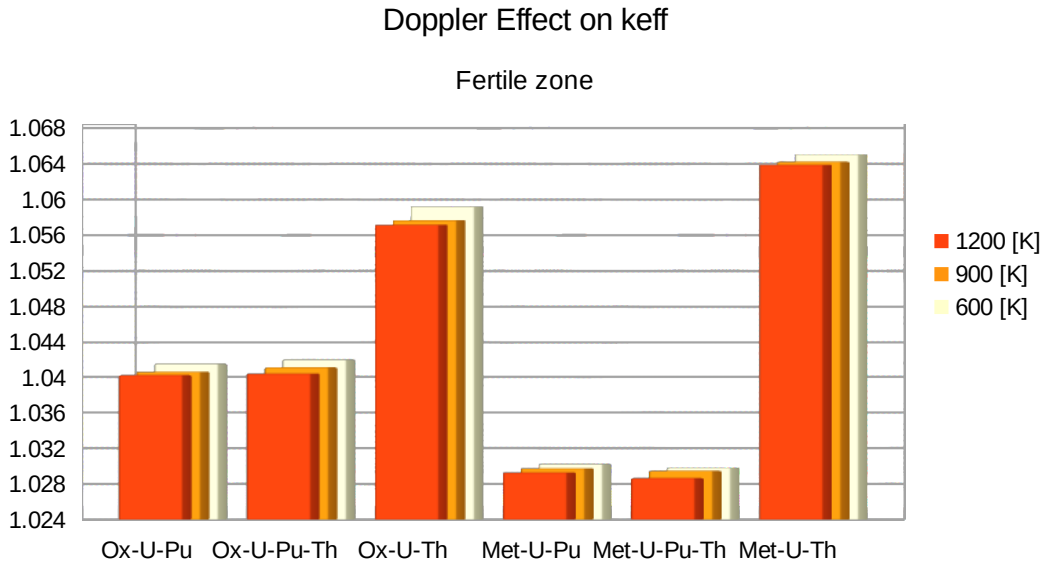

Figure 6.12. Doppler effect on keff (fertile)

Figure 6.13. shows a chart of the calculated value of the Doppler constants of the four cases and the six fuel configurations. It can be seen that in the case of temperature change in the fissile zone, oxide fuels have a better behavior than metallic fuels, especially the Ox-U-Th core. In the case of temperature change in the fertile zone, the resulting Dopppler constant varies more, making a difference of the behavior of the different fuels less conclusive.

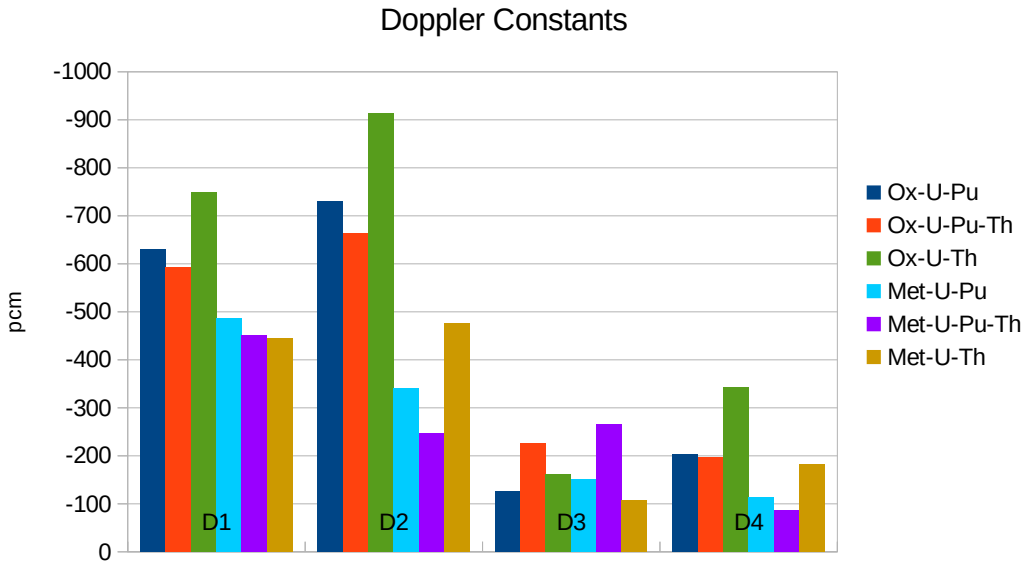

Figure 6.13. Doppler constants

6.5. Reactivity Effect of Coolant Density

Figure 6.14. shows a comparative chart of the obtained values for the reactivity effect of coolant density for all the eighteen cases.

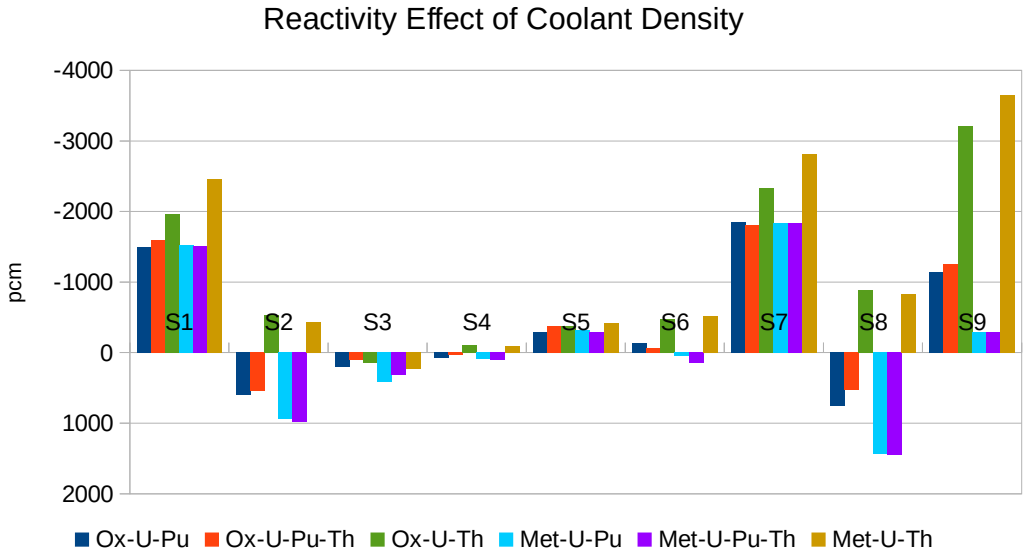

Figure 6.14. Reactivity effect of coolant density

For all the six fuel configurations, the cases S1 and S7 have the best behavior, all of them strongly decreasing the keff value when the coolant density decreases. In the cases S4, S5 and S6, in general all the cores show a negative low void cooling effect constant, which is still good. The cases S3 shows a positive void cooling effect constant, but with low magnitude, and although it is not very bad, it must be taken into account.

The case S9 also shows a negative void cooling effect, being the full $^{232}Th/^{233}U$ fuel configurations the ones with the best behavior for having a more negative void cooling effect; they are followed by

the other two oxide fuel cores, by having lower magnitude constants, but still very good; then the other two metallic fuel cores by having low magnitude constants, but still negative, which is good.

Then we have the cases S2 and S8, showing strong positive void cooling effect constants for all the fuel configurations, except for the full $^{232}Th/^{233}U$ fuel configurations, making these two fuel configurations the best option to face the void coolant effect issue.

6.6. Power Distributions

Figures 6.15. to 6.20. show the radial distribution of power produced by the reactor core. The power of all the assemblies was normalized and it is shown in a color scale, where the assemblies with higher power are shown in red color, the ones with lower power are shown in yellow, and those with no power at all are in black.

All of them show similar behavior, having a ring of the assemblies with the highest power fraction in the outside of the reactor, being these assemblies part of the outer fissile fuel region. The cores with full $^{232}Th/^{233}U$ fuel configurations show more even power distributions.

The highest power peak appears in the Met-U-Pu-Th core fuel, with a value of 1.4317. The lowest power peak appears in the Met-U-Th core fuel, with a value of 1.2693, being this configuration the one with the most even power distribution. These values are at the BoC.

Also, the four diluent assemblies by the center of the core have very low power, as they have few fissile fuel; but this will change along the operating cycle, as these assemblies will breed fissile fuel and will begin to generate more power. This particular point needs further research.

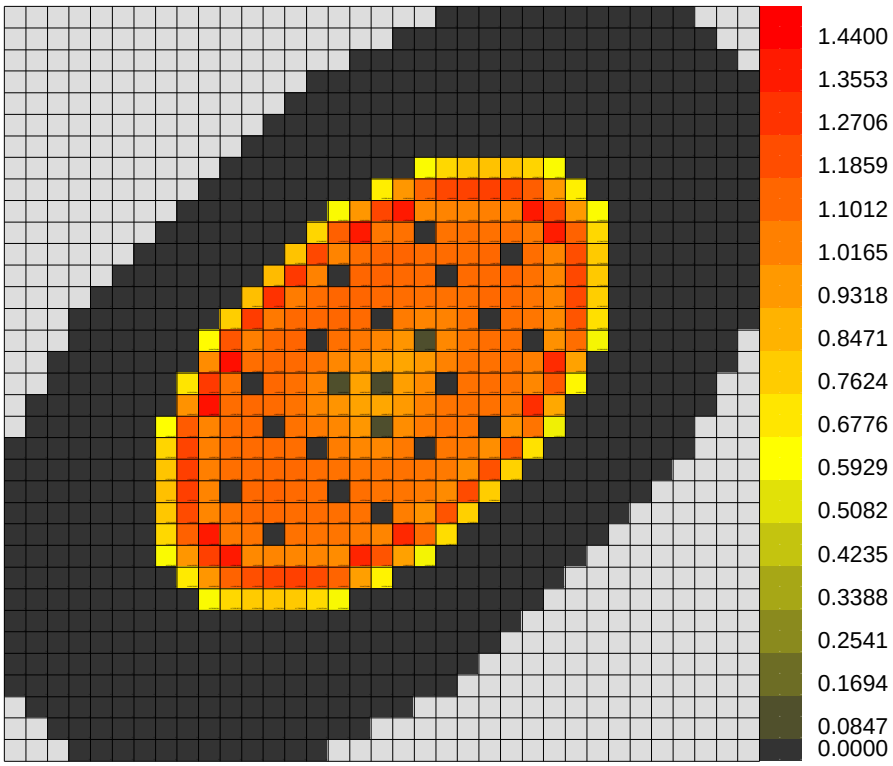

Figure 6.15. Ox-U-Pu radial power distribution

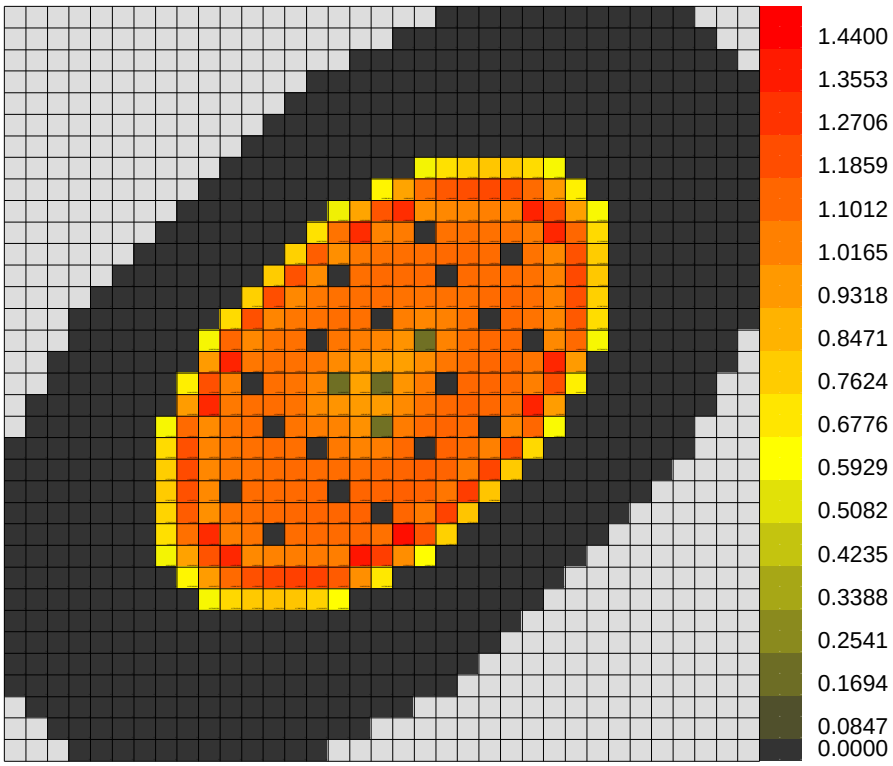

Figure 6.16. Ox-U-Pu-Th radial power distribution

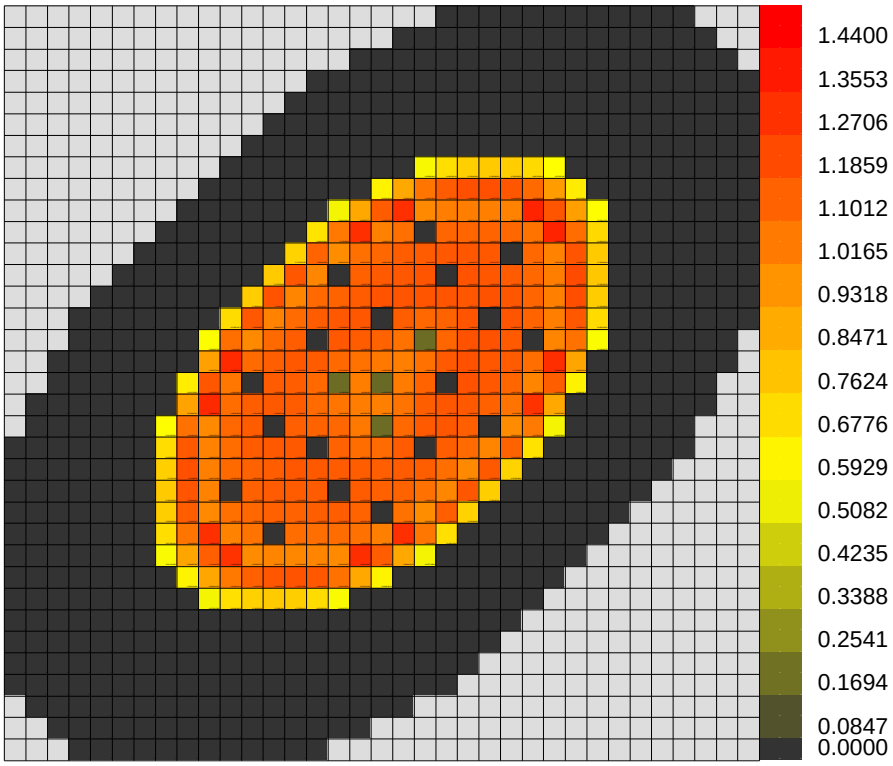

Figure 6.17. Ox-U-Th radial power distribution

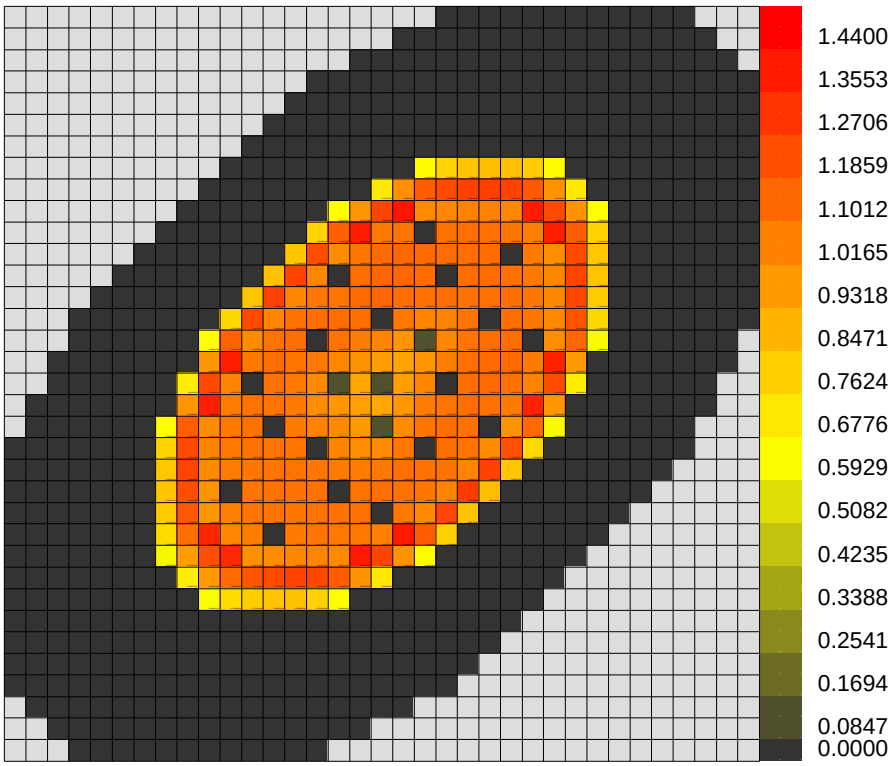

Figure 6.18. Met-U-Pu radial power distribution

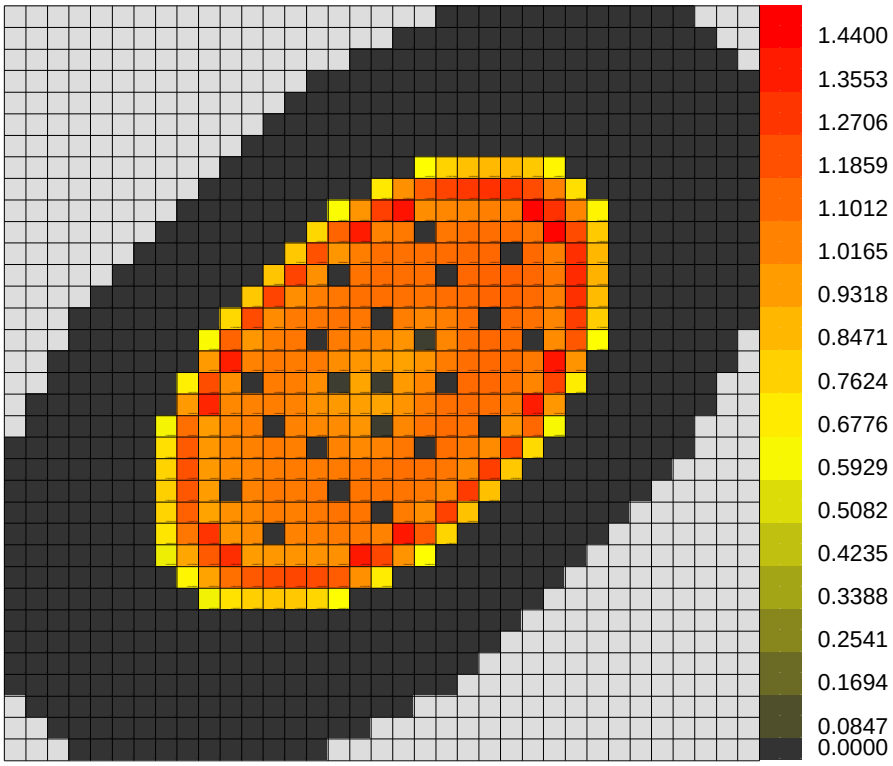

Figure 6.19. Met-U-Pu-Th radial power distribution

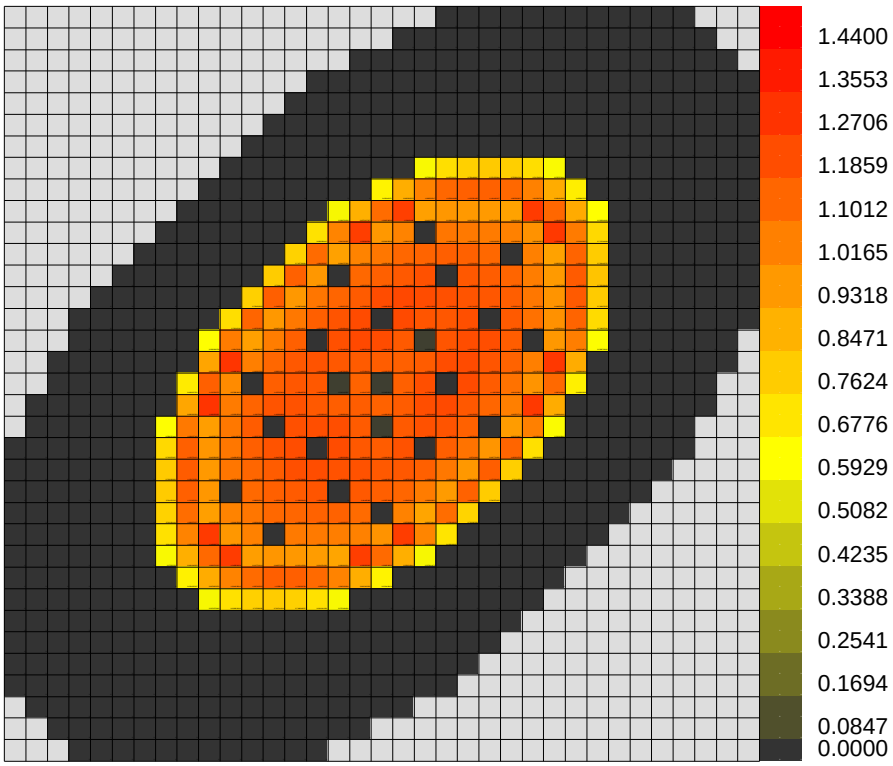

Figure 6.20. Met-U-Th radial power distribution

6.7. Effective Delayed Neutron Fraction β_{eff}

The β_{eff} obtained for the six fuel configurations in [pcm] are as follows:

- Ox-U-Pu = 342.0742
- Ox-U-Pu-Th = 362.1309
- Ox-U-Th = 359.9909
- Met-U-Pu = 404.9841
- Met-U-Pu-Th = 424.4449
- Met-U-Th = 275.3242

In Table 6.1. the fast fission β is shown. As we can see ^{232}Th and ^{238}U have very high values at a fast spectrum, while ^{233}U, ^{235}U and ^{239}U have values similar as those in thermal spectrum.

Nuclide	β (Thermal neutron fission)	β (Fast fission)
^{232}Th	-	0.0203
^{233}U	0.0026	0.0026
^{235}U	0.0065	0.0064
^{238}U	-	0.0148
^{239}Pu	0.0021	0.0020

Table 6.1. Delayed neutron fractions [16]

In the Ox-U-Th, the Met-U-Pu and the Met-U-Pu-Th fuel configurations the β_{eff} is higher because they have a harder spectrum, while in the case of the Met-U-Th the β_{eff} falls because of the stronger influence of the fast fission β of the ^{233}U.

6.8. Shutdown Margin

The keff obtained to know the shutdown margin after changing temperature and inserting all control rods except for the one with the highest integral worth are as follows:

- Ox-U-Pu = 0.95800
- Ox-U-Pu-Th = 0.95755
- Ox-U-Th = 0.96115
- Met-U-Pu = 0.94538
- Met-U-Pu-Th = 0.94234
- Met-U-Th = 0.93091

These values guarantee a SDM > 1% dk/k at the BoC for each one of the six configurations studied here.

7. Conclusions

The ASTRID core model was successfully set up in MCNP6 mainly with the help of the lattice and universe concepts present in the code.

Our ASTRID core model was successfully verified comparing the results with the "*European Benchmark on the ASTRID-like Low-void-effect Core Characterization: Neutronic Parameters and Safety Coefficients*" [13] and with the results reported in: "*A comparison between oxide and metallic ASTRID-like reactors*" [14].

The shutdown margin on each one of the six configurations studied is above 1% dk/k at the BoC, and guarantee a safe shutdown. The effective delayed neutron fraction (βeff) is around 350 [pcm] in the oxide configurations, around 410 for the metallic configurations with plutonium, and 275 for the full ^{232}Th/^{233}U metallic configuration.

The two full ^{232}Th/^{233}U are not good options for the use of thorium in the ASTRID reactor because as both have very hard spectrum, they burn much more fuel than they breed, needing a much higher concentration of fissile ^{233}U than the other configurations. But we must note that they have negative Doppler constant and the best performance in the case of coolant voiding. Also, the Am and Cm isotopes are completely absent along their operating cycle.

The metallic configurations with plutonium have a good performance of the keff along the operating cycle, a lower burden of Am and Cm actinides than the alike oxide configurations, and an acceptable Doppler constant. However, they have the lowest performance in the case of coolant voiding and the higher power peaks.

As a result of this analysis, the best choice at this moment for the use of thorium in the ASTRID reactor is using the Ox-U-P-Th core fuel configuration. It is a good choice because the behavior of the reactor along the cycle of 365 days is very similar to the reference fuel, with slightly different keff at the EoC. The SDM, Doppler constants and the reactivity effect of coolant density are better than the metallic fuel configurations too. It also has a lower burden of Am and Cm actinides than the reference fuel.

Further studies, like a transient analysis and the behavior of the SDM and power distribution along the operating cycle should be performed in order to complement this neutronic study.

References

[1] IAEA. “Nuclear energy, Safe use of nuclear power | IAEA”, https://www.iaea.org/topics/energy (accessed May 14, 2018)
[2] GIF. “GIF Portal, A Technology Roadmap for Generation IV Nuclear Energy Systems”, https://www.gen-4.org/gif/jcms/c_40473/a-technology-roadmap-for-generation-iv-nuclear-energy-systems (accessed May 14, 2018)
[3] GIF Experts Group, “Use of Thorium in the Nuclear Fuel Cycle” (2010).
[4] L. C. Juarez-Martinez and J. L. Francois, “Comparative neutronic study of homogeneous and heterogeneous thorium fuel based core design in a lead-cooled fast reactor”, *Annals of Nuclear Energy*, **114**, 102–109 (2017).
[5] T. Goorley, et al., "Initial MCNP6 Release Overview", Nuclear Technology, 180, pp 298-315 (Dec 2012).
[6] M.B. Chadwick, P. Oblozinský, M. Herman, N.M. Greene, R.D. McKnight, D.L. Smith, P.G. Young, R.E. MacFarlane, G.M. Hale, S.C. Frankle, A.C. Kahler, T. Kawano, R.C. Little, D.G. Madland, P. Moller, R.D. Mosteller, P.R. Page, P. Talou, H. Trellue, M.C. White, W.B. Wilson, R. Arcilla, C.L. Dunford, S.F. Mughabghab, B. Pritychenko, D. Rochman, A.A. Sonzogni, C.R. Lubitz, T.H. Trumbull, J.P. Weinman, D.A. Brown, D.E. Cullen, D.P. Heinrichs, D.P. McNabb, H. Derrien, M.E. Dunn, N.M. Larson, L.C. Leal, A.D. Carlson, R.C. Block, J.B. Briggs, E.T. Cheng, H.C. Huria, M.L. Zerkle, K.S. Kozier, A. Courcelle, V. Pronyaev, S.C. van der Marck: "ENDF/B-VII.0: Next Generation Evaluated Nuclear Data Library for Nuclear Science and Technology," Nucl. Data Sheets, 102, 2931 (2006).
[7] Dr. Franco Michel Sendis; “On thorium as nuclear fuel cycle”*;* OECD Nuclear Fuel Agency (Jul 2017).
[8] Juan Luis Francois, (2008). “El Método de Monte Carlo para la Solución de la Ecuación de Transporte”*;* Lecture notes, School of Engineering, National Autonomous University of Mexico (2008).
[9] Paul J. Atzberger, “The Monte Carlo Method”, https://pdfs.semanticscholar.org/d4a0/df4f34b7e365963ce040d97d52bb79f55ced.pdf (accessed May 14, 2018)
[10] GIF. “GIF Portal – Home – SFR”, https://www.gen-4.org/gif/jcms/c_9361/sfr (accessed May 14, 2018).
[11] CEA – Nuclear Energy Division, “4th Generation Sodium-Cooled Fast Reactors – The ASTRID Technological Demonstrator” (2012).
[12] GIF, “Annual Report 2016” (2016).
[13] S. Bortot, F. Alvarez Velarde, E. Fridman, et. al., “European Benchmark on the ASTRID-like Low-void-effect Core Characterization: Neutronic Parameters and Safety Coefficients”, *Proceedings of ICAPP*, Nice (France), May 03-06, 2015, **15**, 668-676 (2015).
[14] E.-Y.García-Cervantes and J.L.Francois, “A comparison between oxide and metallic fueled ASTRID-like reactors”, *Annals of Nuclear Energy*, **94**, 350–358 (2016).
[15] Charles D. Harmon, Robert D. Busch, Judith F. Briesmeister, R. A. Forster, “Criticality Calculations with MCNP; A Primer”*;* Los Alamos National Laboratory (Aug 1994).
[16] Lamarsh and John R. The time dependent reactor. In *Introduction to Nuclear Engineering*, 2th. ed.; Addison-Wesley Publishing Company: USA, pp 287 (1983).